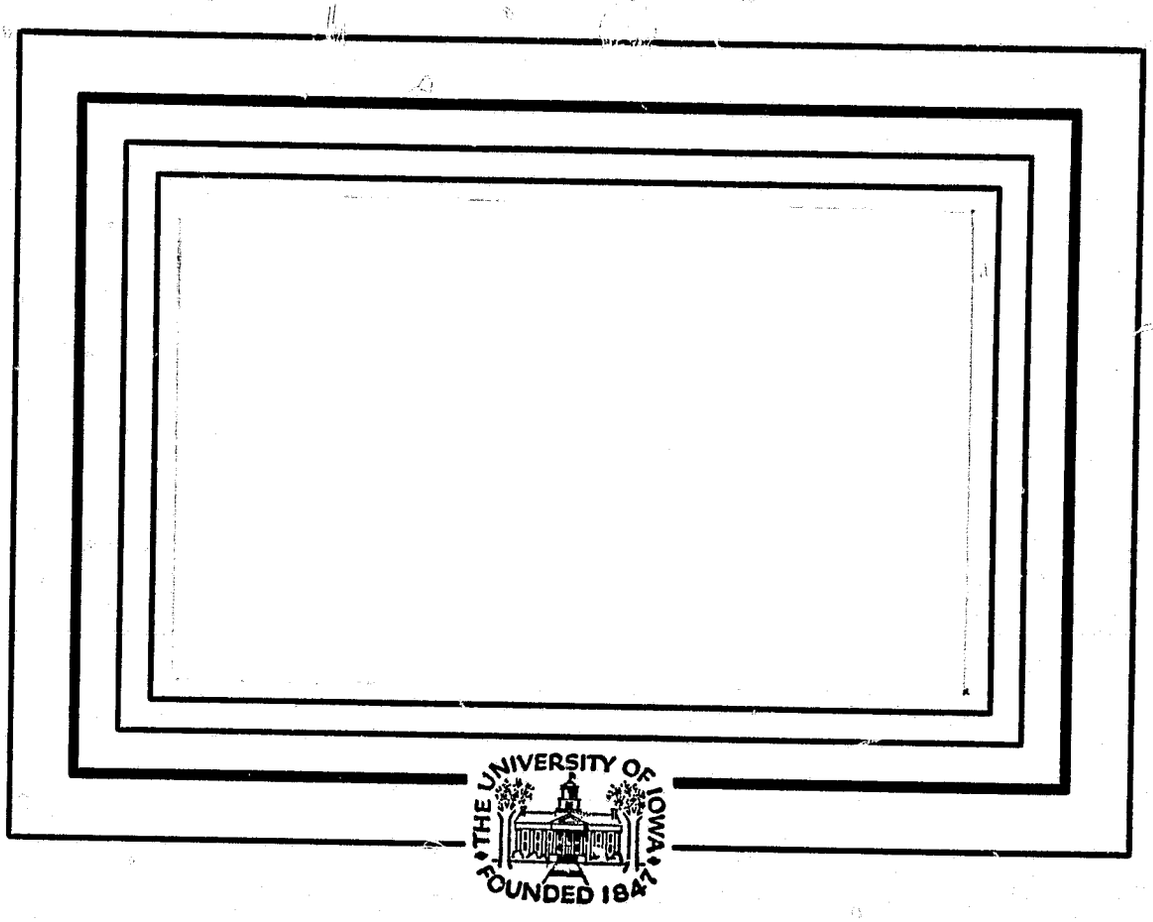

Department of Physics and Astronomy

THE UNIVERSITY OF IOWA

Iowa City, Iowa 52242

U. of Iowa 80-5

Magnetic Pumping of Particles in the Outer Jovian Magnetosphere

by

J. E. BOROVSKY,[1] C. K. GOERTZ,[2]

and G. JOYCE[3]

Department of Physics and Astronomy
The University of Iowa
Iowa City, Iowa 52242

March 1980

[1] Presently at NASA/Goddard Space Flight Center, Planetary Magnetospheres Branch, Greenbelt, Maryland 20771.

[2] Presently at Max-Planck Institut für Aeronomy, Postfach 20, D-3441 Katlenburg, Lindau 3, West Germany.

[3] Presently at JAYCOR, 205 South Whiting Street, Alexandria, Virginia 22304.

ABSTRACT

The mechanism of magnetic pumping consists of two processes, the adiabatic motion of charged particles in a time-varying magnetic field and their pitch-angle diffusion. The result is a systematic increase in the energy of charged particles trapped in mirror (and particularly, magnetospheric) magnetic fields. A numerical model of the mechanism is constructed, compared with analytic theory where possible, and, through elementary exercises, is used to predict the consequences of the process for cases that are not tractable by analytical means. For energy dependent pitch-angle diffusion rates characteristic "two-temperature" distributions are produced.

The model is applied to the outer Jovian magnetosphere for two purposes; to find magnetospheric regions in which the mechanism may energize trapped particles, and to generate distribution functions involving pitch-angle diffusion caused by wave-particle interactions. We find that beyond 20 R_J in the outer magnetosphere particles may be magnetically pumped to energies of the order of 1 - 2 MeV and we predict two-temperature distribution functions with "break points" at 1 - 4 KeV for electrons and 8 - 35 KeV for ions.

INTRODUCTION

Unexpectedly large fluxes of energetic particles were detected in the outer Jovian magnetosphere by the Pioneer and Voyager spacecraft measurements. With energies too high to be explainable by solar-wind injection, the source of these particles is assumed to be within the magnetosphere. One possibility for the energization, proposed by Goertz [1978], is the magnetic-pumping process of Alfvén [1954]. In Alfvén's model [Alfvén and Fälthammar, 1963] cyclic variations of the magnetic field strength are combined with isotropization of the particle distribution functions when the field strength reaches a maximum and/or minimum. As the field strength is increased, the mean perpendicular (to $\vec{B}$) momentum of the distribution increases, conserving the first adiabatic invariant of each particle, while the mean parallel momentum remains constant. Isotropization of the distribution when the field is at a maximum turns some of the high perpendicular momenta into high parallel momenta, which do not decrease when the magnetic field is reduced. Repeating this cycle leads to an increase in the mean momentum of the distribution with time.

Goertz's model is based on the idea that low-energy magnetospheric particles, conserving their total (kinetic plus potential)

energies, will $\vec{E} \times \vec{B}$ drift almost precisely on electric equipotentials. If the magnetic field is not rotationally symmetric, the drift will carry the particles through regions of differing magnetic field strength, hence the magnetic cycle. Pitch-angle scattering of the particles is assumed to be effected by the presence of plasma waves, for example, those observed by the Voyager plasma wave experiment [Gurnett et al., 1979]. One shortcoming of the Goertz model is the requirement that pitch-angle scattering occur only at local noon and midnight. Energization through the magnetic pumping process will also result from various amounts of pitch-angle scattering occurring, more realistically, throughout the magnetosphere. Furthermore, Goertz did not evaluate steady-state distribution functions. Both of these shortcomings will be corrected in this paper although others still remain.

We begin in Section 1 by studying the foundations necessary to model the process of magnetic pumping. We use the conservation of two adiabatic invariants and an assumed shape for the magnetic field to follow the adiabatic motion of particles. In addition, we solve, at each time step, a diffusion equation describing the pitch-angle scattering of particles.

In Section 2 we combine the two devices, adiabatic motion and pitch-angle scattering, to simulate the magnetic-pumping process. We first discuss the theory of the extreme, Alfvénic case, and then complete several exercises for the more realistic case with

pitch-angle diffusion occurring simultaneously with the changing of the mirror magnetic fields. We will identify requirements necessary to make the particle energization most efficient, look at the time behavior of the mean momentum of a group of particles, and examine several distribution functions generated by the mechanism.

In the application to Jupiter, Section 3, we concentrate on predicting the magnetospheric regions in which magnetic pumping may be expected to energize charged particles before they are lost, and on examining distribution functions produced by diffusion coefficients modeled upon resonances with plasma waves. These results pertain to observations made by spacecraft in the Jovian magnetosphere of thus far unexplained energetic particle distributions.

1. ADIABATIC MOTION IN MIRROR GEOMETRY AND DIFFUSION IN PITCH-ANGLE SPACE

Using adiabatic theory, our goal is to follow the evolution in phase space of a distribution function of particles trapped in a magnetic flux tube.

Changes in the field parameters of a flux tube as it convects through a nonsymmetric magnetosphere, or, in the case of mirror machines, as the laboratory magnetic field is altered, will produce distortions of the distribution. We follow separately each element of $n(P,\alpha)$, the number of particles in a flux tube with momentum P and pitch angle α, calculate the new phase space coordinates for each element, and reassemble the distribution. The method used will not require the field to be known for all values of time. Given a distribution in a flux tube with known field parameters, a description of the new field topology will be sufficient to calculate the new distribution.

The coordinate transformations are obtained from the two adiabatic constants of the motion for mirror geometry. An idealized magnetic field topology described below, which although not necessary, will simplify our calculations. The first adiabatic invariant (magnetic moment), μ, may be written

$$\mu = \frac{P_\perp^2}{B} \quad . \tag{1}$$

Using the particle's pitch angle, α ($\alpha = 0°$ for field-aligned velocities), we express the perpendicular momentum of a particle as $P_\perp = P \sin \alpha$, yielding

$$\sin^2 \alpha = \frac{B}{B_m} \quad , \tag{2}$$

where B_m is the mirror field strength. With this equation and the knowledge of a particle's pitch angle at a point of known magnetic field strength, the mirror field strength (independent of particle momenta) can be determined.

The second adiabatic invariant (longitudinal invariant), J, may be written

$$J = \int_0^{z_m} P_\parallel \, dz \quad , \tag{3}$$

where z is the distance along a field line from the equatorial (B = minimum) region. The limits of the integral are thus z = 0 (equator) to $z = z_m$ (mirror point). Writing $P_\parallel$ as $P_\parallel = P\sqrt{1 - \sin^2 \alpha}$ and using Equation (2) to eliminate $\sin^2 \alpha$, this becomes

$$J = P \int_{o}^{z_m} \sqrt{1 - B/B_m}\, dz \tag{4}$$

where $B = B(z)$. Dividing J by $\sqrt{\mu}$, we obtain a hybrid invariant,

$$K = \int_{o}^{z_m} \sqrt{B_m - B}\, dz \quad . \tag{5}$$

We now assume a model for the magnetic field strength, $B(z)$, along a particular flux tube, taking it to be of the form [Goertz, 1978]

$$B = B_o + \frac{1}{2} a z^2 \tag{6}$$

with the restriction that there exists some $z = z_c$ such that

$$B(z_c) = B_c = \text{constant} \tag{7}$$

(see Figure 1). Although this model cannot be regarded as realistic for high latitudes, its analytical convenience is an obvious advantage. We do not expect the qualitative nature of our results to change if we would add higher order terms in Equation (6). We have tested the effect of varying the value of z_c and $B(z_c)$ and have

found no change in energization rates. We also used a square root dependence of B(z) in z and have found little difference in the energization rates.

Inserting the magnetic field model (6) into Equation (5) for the hybrid invariant K, and using Equation (6) to obtain the upper limit of integration, we find

$$K = \frac{\pi}{2\sqrt{2}\ \sqrt{a}} (B_m - B_o) \quad . \tag{8}$$

We are now ready to follow the adiabatic evolution of a distribution function through momentum-pitch-angle space. If the equatorial magnetic field strength is changed from its initial value B_o^{OLD} to a new value B_o^{NEW}, the invariance of $B(z_c)$ in the field model (6) requires

$$a^{NEW} = a^{OLD} + \frac{2(B_o^{OLD} - B_o^{NEW})}{z_c^2} \quad . \tag{9}$$

Thus, for our field model, with any value of a known, the magnetic field for all z is entirely specified by its equatorial value, B_o.

When B_o changes, an element in phase space with equatorial coordinates P^{OLD}, α_o^{OLD} will move to the equatorial coordinates P^{NEW}, α_o^{NEW}. Using the conservation of the hybrid invariant, Equation (8), the particle's new magnetic mirror field strength is found to be

$$B_m^{NEW} = B_o^{NEW} + (B_m^{OLD} - B_o^{OLD}) \sqrt{\frac{a^{NEW}}{a^{OLD}}} \quad , \tag{10}$$

where (Equation (2))

$$B_m^{OLD} = \frac{B_o^{OLD}}{\sin^2 \alpha_o^{OLD}} \quad . \tag{11}$$

Applying Equation (2) in the equatorial region of the new magnetic field with Equation (10) yields an equation for the new equatorial pitch angle in terms of known quantities,

$$\alpha_o^{NEW} = \arcsin\left(\sqrt{\frac{B_o^{NEW}}{B_m^{NEW}}} \right) \quad . \tag{12}$$

The invariance of the magnetic moment, Equation (1), applied at the new and old mirror points yields

$$P^{NEW} = P^{OLD} \sqrt{\frac{B_m^{NEW}}{B_m^{OLD}}} \quad . \tag{13}$$

Thus, our coordinate transformation is obtained as follows. Set the new value for B_o and use Equation (9) to obtain a^{NEW}. Then,

for each point (p^{OLD},α^{OLD}), evaluate Equations (10), (12), and (13) in that order.

The numerical problems of representing the distribution function on a finite phase-space grid is discussed in Appendix I.

The bounce-averaged, pitch-angle diffusion equation for the equatorial particle distribution function $f_o(\alpha_o)$ [Lyons, Thorne, and Kennel, 1972] is

$$\frac{\partial f_o}{\partial t} = \frac{1}{T(\alpha_o)\sin \alpha_o \cos \alpha_o} \frac{\partial}{\partial \alpha_o}\left[T(\alpha_o)\sin \alpha_o \cos \alpha_o \, \mathcal{D}(\alpha_o) \frac{\partial f_o}{\partial \alpha_o}\right] \tag{14}$$

where $T(\alpha_o)$ is the angular dependence of the bounce period and $\mathcal{D}(\alpha_o)$ is a "bounce-averaged" diffusion coefficient. This equation has singularities at $\alpha_o = 0$ and $\alpha_o = \pi/2$ which disappear when we transform it into a diffusion equation for the total number of particles in a flux tube, $n(\alpha_o)$, expressed in terms of equatorial parameters.

If $f_o(\alpha_o)$ is the equatorial distribution function, then

$$f_o(\alpha_o)2\pi \sin \alpha_o \, d\alpha_o = \text{number of particles in the equatorial region with equatorial pitch angles from } \alpha_o \text{ to } \alpha_o + d\alpha_o \; . \tag{15}$$

The extent of the region a particle of given pitch angle α_o and momentum p traverses is twice the distance z_m along the flux tube from the equator (minimum magnetic field) to the mirror point. This may be expressed in terms of $v_{m_{\parallel}}$, the component of a particle's mean velocity parallel to the magnetic field (parallel to the flux tube), as

$$2z_m = \frac{1}{2} \tau_B \, v_{m_{\parallel}} \quad , \tag{16}$$

where τ_B is the bounce period. With the magnetic field model used (Equation (6)), we may show that $v_{m_{\parallel}} = \pi/4 \, v_o \, \cos \alpha_o$, enabling us to write

$$2z_m = \frac{\pi}{8} \tau_B \, v_o \cos \alpha_o \quad . \tag{17}$$

The total number of particles with equatorial pitch angles between α_o and $\alpha_o + d\alpha_o$, $n(\alpha_o)d\alpha_o$, will be the product of the number of particles in the equatorial region with equatorial pitch angles ranging from α_o to $\alpha_o + d\alpha_o$ and the extent of the region they occupy. Thus, from relations (15) and (17), we have

$$n(\alpha_o)d\alpha_o = 2\pi \, \frac{\pi}{8} \, v_o \, f_o(\alpha_o) \tau_B \sin \alpha_o \cos \alpha_o \, d\alpha_o \quad . \tag{18}$$

Using this relation to replace $f_o(\alpha_o)$ in Equation (14) yields

$$\frac{\partial n(\alpha_o)}{\partial t} = \frac{\tau_B}{T(\alpha_o)} \frac{\partial}{\partial \alpha_o} \left[T(\alpha_o) \sin \alpha_o \cos \alpha_o \mathcal{D} \frac{\partial}{\partial \alpha_o} \right.$$

$$\left. \times \left(\frac{n(\alpha_o)}{\tau_B \sin \alpha_o \cos \alpha_o} \right) \right] , \qquad (19)$$

where a factor of $2\pi^2 v_o/8$ has been divided out. We may factor the bounce period τ_B into $T(v_o)T(\alpha_o)$, where $T(v_o)$ and $T(\alpha_o)$ are the velocity and equatorial pitch-angle dependences. On the right-hand side of our equation, the two factors of $T(v_o)$ will cancel, leaving

$$\frac{\partial n(\alpha_o)}{\partial t} = \frac{\partial}{\partial \alpha_o} \left[T(\alpha_o) \sin \alpha_o \cos \alpha_o \mathcal{D}(\alpha_o) \frac{\partial}{\partial \alpha_o} \right.$$

$$\left. \times \left(\frac{n(\alpha_o)}{T(\alpha_o) \sin \alpha_o \cos \alpha_o} \right) \right] . \qquad (20)$$

(This equation may also be derived from first principles by bounce-averaging a Fokker-Planck equation for the diffusion in pitch-angle space [Borovsky, 1980, Chap. III].) Using the product rule on the inner differentiation of (20) and defining

$$H(\alpha_o) = \mathcal{D}(\alpha_o)T(\alpha_o)\sin\alpha_o\cos\alpha_o\frac{\partial}{\partial\alpha_o}\left\{\frac{1}{T(\alpha_o)\sin\alpha_o\cos\alpha_o}\right\}$$

$$= -\mathcal{D}(\alpha_o)\frac{\partial}{\partial\alpha_o}\left\{\log\left[T(\alpha_o)\sin\alpha_o\cos\alpha_o\right]\right\} , \qquad (21)$$

simplifies our diffusion equation to

$$\frac{\partial n(\alpha_o)}{\partial t} = \frac{\partial}{\partial\alpha_o}\left[\mathcal{D}(\alpha_o)\frac{\partial n(\alpha_o)}{\partial\alpha_o}\right] + \frac{\partial}{\partial\alpha_o}\left[H(\alpha_o)n(\alpha_o)\right] . \qquad (22)$$

This diffusion equation describes the pitch-angle scattering in terms of the function $n(\alpha_o)$, the number of particles in a flux tube with equatorial pitch angle α_o. The numerical treatment of Equation (22) is deferred to Appendix I.

2. THEORY AND RESULTS FOR MIRROR GEOMETRY

As a first example of the mirror-geometry energization mechanism we consider Alfvén's model of "magnetic pumping" [Alfvén and Wälthammar, 1963, Sect. 2.7.4]. We follow, in time, a distribution of trapped particles as the equatorial magnetic field is varied from an initial, minimum value of $B_{o_{MIN}}$, to a maximum value $B_{o_{MAX}}$, and returned back to the value $B_{o_{MIN}}$. The model requires that the distribution be diffused to isotropy in pitch-angle space when the field is at its maximum and minimum values. The significant parameter is the ratio k, defined as

$$k = \frac{B_{o_{MAX}}}{B_{o_{MIN}}} \quad . \tag{23}$$

The ratio of the mean momentum of a distribution after one cycle ($B_{MIN} \rightarrow B_{MAX} \rightarrow B_{MIN}$) to the mean initial momentum is

$$\frac{P}{P_o} = \frac{1}{3}\sqrt{5 + 2k + \frac{2}{k}} \quad . \tag{24}$$

Note that, in this model, a value of k = 15.44 will double the momentum (quadruple the energy, nonrelativistically) of the trapped distribution of particles each cycle. In Figure 2 we compare, as a function of the magnetic field ratio k, results of computer simulations of the model to this theoretical prediction for the momenta ratio. The simulations used a 46 x 350 (α_o x P) size grid to represent the particle distribution, and used the $B(z) = B_o + 1/2\ a\ z^2$ magnetic field model in following the adiabatic motion (as B_o and a varied) of the distribution. Attributable to finite grid effects is the fact that the simulations resulted in slightly lower rates of momentum gain than analytical theory predicts. This is due to the boundary conditions requiring the diffusion coefficient $\mathcal{D}$ and its spatial derivative to be zero (see Appendix I) at $\alpha_o = 0, \pi/2$. Thus, the distribution on the end points of our grid does not diffuse with the rest of the distribution. Figure 3 displays the evolution in time of the function $n(P,\alpha_o)$ during one cycle of the Alfvénic model.

We now look into a more applicable, but more complicated, model similar to the one proposed by Murty and Varma [1958]. In the Alfvénic model, the diffusion is restricted to times when the magnetic field is at its maximum and minimum values. At those times, complete isotropization is allowed to occur. In this more realistic model, we require the diffusion to occur continuously, and at a constant rate, as the equatorial field strength changes (sinusoidally)

with time. There are two limiting values of the diffusion rate (amount of diffusion/cycle) for which there will be no momentum gain. The first is the limit of the diffusion rate going to zero. Throughout the cycle the distribution will change adiabatically (no scattering to violate the first or second adiabatic invariant), returning to its original form at the end of a cycle. The second case is the limit of infinite diffusion, forcing the distribution to remain isotropic at all times as the magnetic field varies. Using simple arguments we show in Appendix II that, in this limit, the energization approaches zero.

The results of computer simulations of this model are displayed in Figure 4. Note that there is an optimum diffusion rate producing a maximum in the momentum gain per orbit for a distribution of particles. Murty and Varma describe this maximum as a resonance between the cycle of field variation and the diffusion rate. In Figure 4 we have used the diffusion time $\tau_{DIF} = 0.0738/\Delta$ where the constant 0.0738 is valid for the numerical parameters of our model. This time can be interpreted as the time it would take the lowest eigenfunction of the pitch-angle diffusion operator to decay to 1/e of its initial value for a constant magnetic field. In the case of $k = 3$ ($\beta = 1/2$), we find the ratio of the momentum gain per orbit $(P - P_o)/P_o$ of this model to the momentum gain per orbit of the Alfvén model to be .520 (Murty and Varma predict a ratio of .408).

The magnetic ratio k (= $B_{o_{MAX}}/B_{o_{MIN}}$) dependence of this model is displayed in Figure 2. The diffusion coefficient was chosen so that $\tau_{DIF} = \tau_{CYCLE}$, giving the maximum obtainable momentum gain per cycle.

Of interest in this model is the mean momentum of a particle distribution as a function of time. If, as in Equation (24), we find that after one orbit the mean momentum of the distribution changes according to the relation

$$\frac{P}{P_o} = \text{constant} \quad , \tag{25}$$

then the average value of P as a function of time will be given by [see Alfvén and Fälthammer, 1963]

$$P = P_o \, e^{t/\tau} \tag{26}$$

where $\tau = \tau(B_{o_{MAX}}/B_{o_{MIN}})$ is time- and momentum-independent. In Figure 5 the results of numerical simulations, for two values of $k = B_{o_{MAX}}/B_{o_{MIN}}$, are plotted. The envelope of the k = 3 curve fits the form of Equation (26) quite well, with $P_o = 1.128$ and $\tau = 26.45$ cycles, whereas, the envelope of the k = 10 curve falls below the exponential behavior due to numerical losses off the high-momenta end of the grid.

We now wish to examine steady-state distribution functions produced by the magnetic-pumping process. The first case we investigate is one with the diffusion coefficient constant with momentum (Figure 6), as in our previous models. Particles are produced at a constant rate with low momenta values and are accelerated, on the average, toward higher momenta. Since the diffusion coefficient is constant, with the use of particle flux conservation, we may predict the steady-state shape of the distribution function. The total momentum of a distribution of particles is described by Equation (26), where, since the diffusion coefficient is not a function of momentum, τ is momentum independent. Conservation of particles insures that, as an element of distribution between the low momentum values of P_o and $P_o + \Delta P_o$ moves to higher momentum (and spreads in momentum into P to P + ΔP),

$$f(P_o)\Delta P_o = f(P)\Delta P \quad . \tag{27}$$

Using Equation (26) we see that the low-momentum boundaries of the element move to

$$P_o \rightarrow P = P_o\, e^{t/\tau} \tag{28}$$

and

$$P_o + \Delta P_o \rightarrow P + \Delta P = (P_o + \Delta P_o)e^{t/\tau} \quad , \tag{29}$$

giving

$$\Delta P = \Delta P_o \, e^{t/\tau} \quad . \tag{30}$$

Inserting Equation (30) into the particle flux conservation relation (27) and using Equation (26) to eliminate the exponential, yields

$$f(P) = \frac{f(P_o)P_o}{P} \quad . \tag{31}$$

Thus, the distribution function should be of the form

$$f(P) \propto \frac{1}{P} \quad . \tag{32}$$

The distribution function of Figure 6, with a $P^{-.993}$ falloff, is in excellent agreement with this.

The next cases considered concern diffusion coefficients $\mathcal{D}(P)$ that vary linearly with momentum. Figure 7(a) displays the results of a coefficient variation which produces less efficient energization at higher momenta than it does at lower momenta. As is evidenced in the figure, we may expect particles produced at

low-momenta to "pile-up" as they are accelerated to higher momenta, causing the distribution to fall off slower than 1/P. One interesting consequence of such a diffusion coefficient is the creation of distribution functions with positive slopes. In Figure 7(b) the diffusion coefficient varies in the opposite sense, with the energization being more efficient at higher momenta than at lower. Here, as intuition would indicate, the distribution falls off faster than 1/P.

The final cases of momentum-dependent pitch-angle diffusion coefficients that we choose to examine concern coefficients that vary strongly (or discontinuously) at one momentum value, producing abrupt transitions between (momentum) regions of differing energization efficiencies. The steady-state distribution function of Figure 7(c) bridges the transition between a region of high energization efficiency (at low momenta) and a region of considerably lower efficiency (at high momenta), with only a small effect at the transition momentum. If the diffusion coefficient is such that the regions of energization efficiency are reversed (Figure 7(d)), with low efficiency at low momenta and a sharp transition to high efficiency at high momenta, then a steady-state distribution function that may be interpreted as having "two temperatures" will result. Numerical simulations show that the difference in efficiency across the transition may be small yet still produce a noticeable break in the distribution at that momentum value. "Two-temperature"

distributions are not limited to the steady-state case, but will also evolve from an initial distribution function if particle production is not present.

In this section we have compared (favorably) numerical simulations with theoretical predictions for the Alfvénic model of magnetic pumping and have completed elementary exercises for the continuous-diffusion magnetic-pumping model, finding a maximum energization occurring at a "resonance" between the diffusion- and magnetic cycle-times, and explored the distribution functions generated by the process when the pitch-angle diffusion rate is allowed to be a function of particle momentum. We now apply the continuous-diffusion magnetic-pumping mechanism to particles trapped in the corotating magnetosphere of Jupiter.

3. PARTICLES IN THE JOVIAN MAGNETOSPHERE

Due to the azimuthal asymmetry of the Jovian magnetic field, particles will drift around the planet through regions of differing magnetic field strength, and due to the presence of plasma waves, those particles will be pitch-angle scattered as they drift. Thus, for particle distributions trapped in the magnetosphere, there exist mechanisms both for changing the magnetic field strength (adiabatic motion) and for pitch-angle scattering (diffusion).

We first determine the regions (if any) of the magnetosphere in which the energizing mechanism may be applicable. In order to model the equatorial magnetic field strength and to calculate the corotational electrical potentials of Jupiter, we choose [as in Goertz, 1978] the Barish-Smith [1975] magnetic field model for the compressed dayside magnetosphere and the Goertz et al. [1976] model for the nightside magnetotail. (See Figure 8.) It is assumed that for distances less than 20 R_J ($R_J \approx 7.10^9$ cm) the Jovian magnetic field is approximately dipolar, whereas the nightside model falls considerably below the proper dipolar values close to the planet. Hence, we shall apply our model only in the outer magnetosphere (beyond $r = 20\ R_J$) and assume the magnetotail model matches a dipole field somewhere within 20 R_J. Although these field models are

idealized we believe that they represent the important features of the asymmetric Jovian magnetosphere.

The equatorial electric potentials (Figure 9) were obtained by integrating the corotational electric fields from r = ∞ to the position of interest, that is

$$V = \int_{\infty}^{r} \frac{1}{c} (\vec{v} \times \vec{B}) dr \quad , \tag{33}$$

where we will assume that the magnetosphere corotates in the region of interest (20 - 50 R_J). For the magnetotail model, integral (33) is written

$$V_{TAIL} = - \frac{\Omega}{c} \int_{\infty}^{r} r \left[\frac{M}{r^3} - \frac{M'}{r^{2.7}} \right] dr + \text{constant} \quad , \tag{34}$$

where the constant shifts the potential to match, at r = 20 R_J, the corotational electric potential of a dipole. Integrating, we find (r in cm)

$$V_{TAIL} = \frac{\Omega}{c} \left[\frac{M}{r} - \frac{M'}{r^{.7}} \right] - \frac{\Omega}{c} \frac{M}{20\ R_J} \quad , \tag{35}$$

where,

$$\Omega = 1.77 \times 10^{-4}/\text{sec}$$

$$M = 4.225 \text{ gauss } R_J^3 = 1.449 \times 10^{30} \text{ gauss cm}^3$$

$$M' = .63 \text{ gauss } R_J^{2.7} = 2.4 \times 10^{26} \text{ gauss cm}^{2.7} \quad . \qquad (36)$$

The dayside corotational electric potentials are more difficult to obtain since the Barish-Smith magnetic field model equations must be solved by iteration at every position in space, hence the equatorial electric potentials were obtained by numerical integration (and again, the potential was matched to dipolar values at $r = 20\ R_J$).

As charged particles drift in the magnetosphere, their total energy (kinetic plus electric potential) is conserved. For low energy particles (with much less kinetic energy than electrical potential), the drift is along equipotential surfaces. Hence, as a function of frontside radii, we may calculate the tailside drift radii and the front- and tailside equatorial magnetic field values. Knowing the front (maximum) and tail (minimum) magnetic field strengths gives us the ratio k (relation (23)), as a function of r (frontside), plotted in Figure 10. With k(r), we are in a position to claculate the "energization time" of a distribution as a function of the frontside radius. We define the energization time τ_E to be the time, in number of Jovian rotations, that it takes to double the mean (nonrelativistic) energy of a distribution of trapped particles. Numerically simulated values of τ_E for the continuous

diffusion model with various (α_o-independent) diffusion coefficients are plotted as functions of dayside radius in Figure 11. Energization times for the Alfvénic model (giving the fastest possible energization for magnetic pumping) are plotted for comparison.

To determine the regions of the magnetosphere in which the pumping mechanism energizes particles, we must compare the energization time τ_E to particle loss times. In the outer magnetosphere loss cone escape of particles is negligible [Coroniti, 1975]. We use the following value for the "normal" radial diffusion coefficient in the outer magnetosphere [Coroniti, 1975]

$$D_{LL}\Big|_{M,J} = 2 \times 10^{-10}\ L^3/\text{sec} \quad , \tag{37}$$

to estimate the radial diffusion loss time (see discussion below),

$$\tau_{RD} = \left[\frac{1}{B}\frac{\partial B}{\partial r} D_{LL} \frac{1}{f}\frac{\partial f}{\partial r}\right]^{-1}_{M,J} \cong \left[\frac{1}{B}\frac{\partial B}{\partial r} D_{LL} \frac{1}{1\ R_J}\right]^{-1}_{M,J} \quad . \tag{38}$$

The result is the curve in Figure 11. Particles are energized in regions where the energization time τ_E is less than the radial diffusion loss time τ_{RD}. Note that the disclosure of energizing regions is very sensitive to the estimate of the radial diffusion coefficient, which, if estimated to be a factor of ten higher than

the value assumed, will lead to the prediction of no particle energization in the 20 - 50 R_J region examined.

Energy conservation for a drifting particle yields an upper limit to the kinetic energy that a particle may gain through the magnetic-pumping process. A low energy particle will $\vec{E} \times \vec{B}$ drift on an orbit which lies on an electrical equipotential surface, the drift carrying the particle through regions of differing magnetic field strength, hence the possibility of it being magnetically "pumped". A high energy particle will drift on a surface of constant magnetic field strength, eliminating the possibility of further magnetic pumping. To estimate this kinetic energy limit, we calculate the difference in electrical potential, ΔV, along a drift orbit which lies on a surface of a constant magnetic field and assume that the magnetic-pumping process will give energy to a particle as long as it has a kinetic energy

$$W < q\,\Delta V \quad . \tag{39}$$

For all B = constant drift orbits in the region from 25 R_J to 45 R_J, we find that $\Delta V \cong 2$ MeV, so, for the magnetic field models chosen, the magnetic-pumping mechanism may, in that region, energize particles (ions and electrons) up to energies of at least 1 MeV.

An increase in kinetic energy due to the magnetic-pumping process will correspond to a radial transport of particles. The

total energy (kinetic plus electrical potential) being constant, the change in kinetic energy is related to a change in the potential energy by

$$\Delta W = - qE \, \Delta r \quad . \tag{40}$$

Using $E = - \Omega \, r \, B/c$ for the corotational electric field, and dividing by Δt, relation (40) is rewritten

$$\frac{\partial W}{\partial t} = \frac{q \, \Omega \, r \, B}{c} \frac{\partial r}{\partial t} \quad , \tag{41}$$

giving the radial velocity of the transport,

$$v_r = \frac{c}{q \, \Omega \, r \, B} \frac{\partial W}{\partial t} \quad . \tag{42}$$

Knowing $W = P^2/2m$, we may write Equation (26) in terms of an energization time, τ_E, as

$$W = W_o \, e^{t/\tau_E} \quad . \tag{43}$$

enabling us to replace the derivative in Equation(42), yielding the radial transport velocity

$$V_r = \frac{c\,W}{q\,\Omega\,r\,B\,\tau_E} \quad . \tag{44}$$

Note that, for energization, this corresponds to an outward (toward larger r) flow of ions and an inward flow of electrons.

If we assume that, for any particle in a distribution function, the chances of being energized or de-energized during a cycle of the process are equal, then the radial displacements Δr of a particle have zero mean and the radial transport may be described as a diffusion process. To approximate the radial diffusion coefficient we write

$$D_{LL}\Big|_E = \frac{\langle (\Delta L)^2 \rangle}{\tau_R} \tag{45}$$

where $\Delta L \cong R_J\,\Delta r$ and $\tau_R = 3.57 \times 10^4$ sec is the Jovian rotational period. We obtain ΔL from relation (40) and approximate the change in kinetic energy during one cycle by $\Delta W \cong \partial W/\partial t\ \tau_R$ with Equation (43), yielding

$$D_{LL}\Big|_E \cong \frac{W^2\,\tau_R}{q^2 E^2 R_J^2 \tau_E^2} \tag{46}$$

or, replacing the corotational electric field E,

$$D_{LL}\Big|_E \cong \left(\frac{W}{B\, r\, \tau_E}\right)^2 \frac{\tau_R\, c^2}{q^2 \Omega^2 R_J^2} \quad . \tag{47}$$

This type of radial diffusion preserves the total energy but not the first or second adiabatic invariants.

Our treatment neglects the displacement of particles in the radial direction which is a necessary consequence of the pumping process. However, if the displacement ΔL in one rotation period is small ($\Delta L/L \ll 1$) our results should accurately describe the local change of characteristic energy. Particles can also diffuse radially by flux tube interchange motion or "normal" L shell diffusion conserving the first and second adiabatic invariant. If this process is faster than the L shell diffusion at constant total energy the adiabatic deceleration of outwardly diffusing particles will be greater than the energy gain by magnetic pumping. The characteristic energy of the plasma ions in the Jovian magnetosphere will decrease with increasing distance in those regions where L shell diffusion at constant first and second adiabatic invariant is faster than the L shell diffusion at constant total energy. "Normal" L shell diffusion can be viewed as a loss of particles at constant energy (for outward diffusion and a spectrum that decreases with energy), and its strength can be characterized by a loss time given by Equation (38).

For completeness, we look briefly at the pitch-angle distribution functions of particles (ions and electrons) corotating with the Jovian magnetosphere. The cases we choose to display concern $k = B_{o_{MAX}}/B_{o_{MIN}} = 4$ orbits where, in one case the particles experience continuous diffusion (Figure 12(a)), and in the other case experience increased amounts of diffusion in differing regions of their orbits (Figure 12(b)). All cases are associated with pitch-angle-independent diffusion coefficients. By comparison with measured Jovian pitch-angle distributions, these computer-generated distributions may be useful for estimating the absolute amounts (Figure 12(a)) of and spatial (local time) dependencies (Figure 12(b)) of the actual diffusion coefficients.

In order to predict distribution functions in the Jovian magnetosphere, we construct a more realistic (pitch-angle and momentum-dependent) diffusion coefficient, describing whistler-mode scattering of electrons and ion cyclotron scattering of ions. The pitch-angle dependence is modeled after the terrestrial electron bounce-averaged diffusion coefficient of Lyons, Thorne, and Kennel [1972, Figure 4], where the diffusion of large pitch-angle particles is due to Landau resonance with the waves and diffusion of small pitch-angle particles is due to cyclotron harmonic resonances. To this diffusion coefficient we add a smooth low-momentum cutoff of the cyclotron resonance contribution (see Figure 2, top, of Lyons, Thorne, and Kennel). To estimate the electron and ion velocities

at this cutoff, we use the Doppler-shifted cyclotron-resonance condition

$$\omega - k_{\parallel} v_{\parallel} = \frac{N\Omega}{\gamma} \quad , \tag{48}$$

where

ω, k = frequency and wave number of wave

Ω = cyclotron frequency for relevant species

v = particle velocity

$$\gamma = \left[1 - \frac{v^2}{c^2}\right]^{-1/2}$$

N = order of resonance .

Choosing the whistler-mode frequency to be $\omega = 1/10\ \Omega$ and the ion-cyclotron-mode frequency to be $\omega = 1/10\ \Omega_i$, we find, for $N = -1$, the critical velocities to be, for electrons,

$$v_c = \frac{1.1\sqrt{10}}{\sqrt{4\pi m_e}} \frac{B}{\sqrt{n_o}} \quad , \tag{49}$$

and for ions,

$$v_c = 11\, v_{ALFVÉN} = 11 \frac{B}{\sqrt{4\pi n_o A m_p}} \quad , \tag{50}$$

where,

n_o = plasma density

$m_{e,p}$ = mass of electron, proton

A = atomic number of dominant ion species .

In the vicinity of 50 R_J ($B = 2 \times 10^{-5}$ gauss), we use the plasma density limits of Barbosa et al. [1979], $n_o = .035\ cm^{-3} - .14\ cm^{-3}$, and find that the resonance cutoffs correspond to electron kinetic energies of from 1 KeV to 4 KeV and to ion kinetic energies of from 8 KeV to 35 KeV, regardless of the species of the dominant ions. For both electrons and ions, the cutoff energies vary as B^2/n_o. Our diffusion coefficient is displayed in Figure 13.

The distribution functions, both steady-state and time evolving, are of the "two-temperature" type with break points occurring near the cyclotron-resonance cutoff. A steady-state case is displayed in Figure 14(a) where particles are produced with momentum values below the cyclotron resonance cutoff transition region and are accelerated (on the average) to higher momenta. The distribution function maintains this "two-temperature" character through the extent of its orbital travel. This "two-temperature"

trait is omnidirectional; i.e., examination of the distribution function (f vs p) for any pitch angle will yield a similar shape. Figure 14(b) concerns the time development of a distribution under the action of our wave-particle diffusion coefficient. The double-temperature character sets in promptly (more rapidly if the diffusion is increased). In this case, as in the steady-state case, the distribution function's traits are omnidirectional.

4. SUMMARY AND DISCUSSION

We have extended the original model of Goertz [1978] to treat, under more realistic assumptions, the evolution of particle distribution functions in the Jovian magnetosphere. The model of Goertz assumed pitch-angle diffusion to occur only in certain regions of the Jovian magnetosphere (i.e., noon and midnight) and corresponds to the old model of Alfvén [1954]. In reality pitch-angle diffusion must take place in all regions of the magnetosphere, although its strength may be local-time dependent. We have numerically followed the evolution of an arbitrary distribution function assuming that all particles stay on one drift shell. This is not exactly true but a reasonable approximation for energies below 1 MeV. In the magnetic-pumping process the characteristic energy (mean energy) of the distribution increases exponentially with time and we have investigated the time constant τ_E of this increase as a function of magnetic field topology and pitch-angle diffusion strength. It should be stressed that as the mean energy increases the particles spread in real space, the radial diffusion being directly related to the pitch-angle diffusion strength and the field topology via τ_E. The mechanism does therefore not increase the total energy content of a flux tube if the plasma distribution is

uniform in space. However, if particles are injected in the inner region of Jupiter, the characteristic energy and energy distribution of the plasma varies with radial distance. If τ_E is smaller than the time for radial diffusion at constant first and second adiabatic invariants, the characteristic energy for ions increases with distance, and for electrons, decreases with distance. Otherwise it decreases for ions and increases for electrons, but not as fast as expected on the basis of conservation of the first two adiabatic invariants. We will discuss this point in more detail in a future paper.

We now will discuss the global aspects of our results. It is believed [Goertz, 1979; Hill, 1979] that Io is the main source of plasma in the Jovian magnetosphere, injecting ions at a considerable rate (10^{28} ... 10^{29} ions/sec). These maintain the "torus". However, fluctuating fields will allow the torus ions to diffuse radially outwards (and inwards). Due to the azimuthal symmetry of the magnetosphere, within 20 R_J the magnetic-pumping time scale τ_E is very long and radial diffusion should preserve the first and second adiabatic invariants. The plasma temperature should thus decrease with radial distance out to about 20 R_J, although not as fast as r^{-3}. Beyond 20 R_J the magnetic pumping becomes effective due to the azimuthal distortion of the magnetic field and the characteristic energy of the ions should increase with radial distance. The energy spectrum of charged particles should be as shown in

Figure 14(a,b) with the break point occurring near 20 keV at 50 R_J. This spectrum is in agreement with that suggested by Belcher et al. [1980]. We regard Figure 14(a,b) as the major new result of this work.

A careful reader will have noticed that the magnetic pumping energizes only inward diffusion electrons. Magnetic pumping causes ions to diffuse outwards and electrons inwards. This constitutes a radial current which has to be closed if a steady-state rotation is to be maintained. We suggest that the current is closed by field-aligned currents carried by electrons out of the Jovian ionosphere. This is also implied in the model of Hill [1979] and has been suggested by us before [Goertz, 1979]. The ionospheric electrons can be trapped in the equatorial current sheet [Goertz, 1973, 1976] and provide a source for inwardly diffusing electrons which are strongly heated as they are transported. We will elaborate on these aspects in a future paper. In Figure 15 we give an overview of this model and sketch the expected distributions for electrons and ions at various locations in the magnetosphere.

APPENDIX I

NUMERICAL TREATMENT OF ADIABATIC MOTION AND DIFFUSION

Using the results of Section 1, we may follow the adiabatic motion through phase space of any particle of a distribution trapped in a time-varying magnetic flux tube. An element of distribution at the old coordinates, (P^{OLD},α_o^{OLD}), is assigned to the new coordinates (P^{NEW},α_o^{NEW}), that is, $n(P^{NEW},\alpha_o^{NEW}) = n(P^{OLD},\alpha_o^{OLD})$. Numerically, we represent the old distribution function $n(P^{OLD},\alpha_o^{OLD})$ on a finite grid in (P,α_o) phase space, assigning a certain fraction of the distribution to each grid point. After the magnetic field is changed, we will find that, in general, unlike the old phase space coordinates, the new coordinates (P^{NEW},α_o^{NEW}) will not fall on grid points. Hence, a method of assigning the distribution $n(P^{NEW},\alpha_o^{NEW})$ to the grid points near the position (P^{NEW},α_o^{NEW}) must be obtained. The scheme used divides the distribution between the four grid points forming the rectangle containing the point (P^{NEW},α_o^{NEW}). Let $P^{NEW} = P_c + v$ and $\alpha_o^{NEW} = \alpha_c + u$ (see Figure 16). The simple scheme chosen is

$$n(P_c,\alpha_c) = (1 - g)(1 - h)n(P^{NEW},\alpha_o^{NEW})$$

$$n(P_c,\alpha_{c+1}) = g(1 - h)n(P^{NEW},\alpha_o^{NEW})$$

$$n(P_{c+1},\alpha_c) = (1 - g)h\ n(P^{NEW},\alpha_o^{NEW})$$

$$n(P_{c+1},\alpha_{c+1}) = g\ h\ n(P^{NEW},\alpha_o^{NEW}) \qquad (A.1)$$

where $g = g(u)$ and $h = h(v)$. Note that this division conserves the number of particles

$$n(P_c,\alpha_c) + n(P_c,\alpha_{c+1}) + n(P_{c+1},\alpha_c)$$
$$+ n(P_{c+1},\alpha_{c+1}) = n(P^{NEW},\alpha_o^{NEW}) \quad . \qquad (A.2)$$

We will choose $g(u)$ and $h(v)$ such that scheme (A.1) conserves two further quantitites, P^2 and α_o. These choices were found to give the greatest accuracy in reproducing a transformed-untransformed distribution function. Solving the P^2 conservation equation

$$P^{NEW^2}\ n(P^{NEW},\alpha_o^{NEW}) = P_c^2\ n(P_c,\alpha_c) + P_c^2\ n(P_c,\alpha_{c+1})$$
$$P_{c+1}^2\ n(P_{c+1},\alpha_c) + P_{c+1}^2\ n(P_{c+1},\alpha_{c+1}) \qquad (A.3)$$

and the α conservation equation

$$\alpha_o^{NEW}\, n(P^{NEW},\alpha_o^{NEW}) = \alpha_c\, n(P_c,\alpha_c) + \alpha_{c+1}\, n(P_c,\alpha_{c+1}) + \alpha_c\, n(P_{c+1},\alpha_c) + \alpha_{c+1}\, n(P_{c+1},\alpha_{c+1}) \qquad (A.4)$$

with the insertion of relations (A.1) yield, respectively,

$$h = \frac{P^{NEW^2} - P_c^2}{P_{c+1}^2 - P_c^2} \qquad (A.5)$$

and

$$g = \frac{\alpha_o^{NEW} - \alpha_c}{\alpha_{c+1} - \alpha_c} \qquad (A.6)$$

or

$$g = u \quad . \qquad (A.7)$$

Another method may be used to follow the adiabatic transformation in phase space of the distribution function. At each grid point of the new coordinates (P^{NEW},α_o^{NEW}), we look back in time on the old (P^{OLD},α_o^{OLD}) grid to ask where the element of distribution $n(P^{NEW},\alpha_o^{NEW})$ came from. Unlike (P^{NEW},α_o^{NEW}), the source point

(P^{OLD},α_o^{OLD}) did not lie on a grid point, and $n(P^{OLD},\alpha_o^{OLD})$ must be estimated by an interpolation. Interpolation schemes using up to 34 points on the (P^{OLD},α_o^{OLD}) grid were tried, and two drawbacks were found to make the method unacceptable. The distribution function was not conserved in the transformation and, more hindering, the magnetic field had to be changed slowly in time in order to prevent large shape changes in the distribution function which introduced errors in the interpolation scheme.

For numerical treatment of the pitch-angle diffusion Equation (22), we center it in time (implicit scheme), writing a set of equations

$$\frac{n_i^{N+1} - n_i^N}{\Delta t} = \frac{\partial}{\partial \alpha_o}\left[\mathcal{D}\,\frac{\partial n}{\partial \alpha_o}\right]_i^{N+1/2} + \frac{\partial}{\partial \alpha_o}\,[H\,n]_i^{N+1/2} \quad , \tag{A.8}$$

where the superscripts (subscripts) represent the time (pitch-angle) grid points. The pitch-angle derivatives will be represented as

$$\frac{\partial}{\partial \alpha_o}\left[\mathcal{D}\,\frac{\partial n}{\partial \alpha_o}\right]_i = \frac{1}{\Delta\alpha}\left[\mathcal{D}_{i+1/2}\,\frac{\partial n_{i+1/2}}{\partial \alpha_o} - \mathcal{D}_{i-1/2}\,\frac{\partial n_{i-1/2}}{\partial \alpha_o}\right]$$

$$= \frac{1}{2(\Delta\alpha)^2}\,[n_{i+1}(\mathcal{D}_{i+1} + \mathcal{D}_i) + n_i(-\mathcal{D}_{i+1} - 2\mathcal{D}_i - \mathcal{D}_{i-1}) + n_{i-1}(\mathcal{D}_i + \mathcal{D}_{i-1})] \quad , \tag{A.9}$$

and

$$\frac{\partial}{\partial \alpha_o}\,[H\ n]_i = \frac{\partial H_i}{\partial \alpha_o}\,n_i + H_i\,\frac{\partial n_i}{\partial \alpha_o}$$

$$= \frac{1}{2\Delta\alpha}\,[n_{i+1}\,H_i + n_i(H_{i+1} - H_{i-1}) + n_{i-1}(-H_i)] \quad . \tag{A.10}$$

Centering these in time about the point N + 1/2 (we use $n^{N+1/2} = 1/2\ n^{N+1} + 1/2\ n^N$), and inserting them into Equation (A.8) yields

$$n_{i+1}^{N+1}\{-\varkappa(\mathfrak{D}_{i+1} + \mathfrak{D}_i) - \varkappa\,\Delta\alpha\,H_i\} + n_i^{N+1}\{1 + \varkappa(\mathfrak{D}_{i+1} + 2\mathfrak{D}_i + \mathfrak{D}_{i-1}) - \varkappa\,\Delta\alpha(H_{i+1} - H_{i-1})\} + n_{i-1}^{N+1}\{-\varkappa(\mathfrak{D}_i + \mathfrak{D}_{i-1}) + \varkappa\,\Delta\alpha\,H_i\}$$

$$= n_{i+1}^{N}\{\varkappa(\mathfrak{D}_{i+1} + \mathfrak{D}_i) + \varkappa\,\Delta\alpha\,H_i\} + n_i^{N}\{1 + \varkappa(-\mathfrak{D}_{i+1} - 2\mathfrak{D}_i - \mathfrak{D}_{i-1}\} + n_{i-1}^{N}\{\varkappa(\mathfrak{D}_i + \mathfrak{D}_{i-1}) - \varkappa\,\Delta\alpha\,H_i\} \quad , \tag{A.11}$$

where we have defined

$$\varkappa = \frac{\Delta t}{4(\Delta\alpha)^2} \quad . \tag{A.12}$$

The implicit scheme (A.11) may be written in tridiagonal form

$$a_i \, n_{i+1}^{N+1} + b_i \, n_i^{N+1} + c_i \, n_{i-1}^{N+1} = d_i \qquad \text{(A.13)}$$

where

$$a = C_1 - \varkappa \, \Delta\alpha \, H_i$$

$$b = 1 + C_2 - \varkappa \, \Delta\alpha (H_{i+1} - H_{i-1})$$

$$c = C_3 + \varkappa \, \Delta\alpha \, H_i$$

$$d = t_1 \, n_{i+1}^{N} + t_2 \, n_i^{N} + t_3 \, n_{i-1}^{N} \quad , \qquad \text{(A.14)}$$

and

$$C_1 = - \varkappa (\mathcal{D}_{i+1} + \mathcal{D}_i)$$

$$C_2 = \varkappa (\mathcal{D}_{i+1} + 2\mathcal{D}_i + \mathcal{D}_{i-1})$$

$$C_3 = - \varkappa (\mathcal{D}_i + \mathcal{D}_{i-1})$$

$$t_1 = - C_1 + \varkappa \, \Delta\alpha \, H_i$$

$$t_2 = 1 - C_2 + \varkappa \, \Delta\alpha (H_{i+1} - H_{i-1})$$

$$t_3 = - C_3 - \varkappa \, \Delta\alpha \, H_i \quad . \qquad \text{(A.15)}$$

Before looking at the algorithm used to solve the diffusion equation, we examine the necessary boundary conditions. The

requirement that the total number of particles in the flux tube be constant may be expressed

$$\int_0^{\pi/2} \frac{\partial n(\alpha_o)}{\partial t} \, d\alpha_o = 0 \quad , \tag{A.16}$$

or, using Equation (22), as

$$\left[\mathcal{D} \frac{\partial n}{\partial \alpha_o} \right]_{\alpha_o=0}^{\pi/2} + \left[H \, n \right]_{\alpha_o=0}^{\pi/2} \quad : \tag{A.17}$$

This we may satisfy by requiring $\mathcal{D}(\alpha_o)$ and $n(\alpha_o)$ to vanish at the boundaries, $\alpha_o = 0, \pi/2$. Note that $n(\alpha_o)$ being zero for pitch angles 0 and $\pi/2$ is consistent with the expression (18) relating $n(\alpha_o)$ to the distribution function $f_o(\alpha_o)$. To insure that $n(\alpha_o)$ remain zero on the boundaries for all times, we constrain $\partial n(0)/\partial t$ and $\partial n(\pi/2)/\partial t$ to be zero. Applying Equation (22) at the two boundaries, we see that

$$0 = \frac{\partial \mathcal{D}}{\partial \alpha_o} \frac{\partial n}{\partial \alpha_o} + \mathcal{D} \frac{\partial^2 n}{\partial \alpha_o^2} + \frac{\partial H}{\partial \alpha_o} n + H \frac{\partial n}{\partial \alpha_o} \quad , \quad \alpha_o = 0, \frac{\pi}{2} \quad . \tag{A.18}$$

This is satisfied by insisting that $\partial \mathcal{D}/\partial \alpha_o$, $\mathcal{D}(\alpha_o)$ (already required), $n(\alpha_o)$ (already required), and $H(\alpha_o)$ (consistent with definition (21)) all vanish at the boundaries $\alpha_o = 0$ and $\alpha_o = \pi/2$.

We now examine the simple tridiagonal algorithm used to solve the set of diffusion equations (A.13) (see, for example, Roache [1972], Appendix A), consistent with the above boundary conditions. We assume there exist solutions of the form

$$n_i^{N+1} = e_i \, n_{i+1}^{N+1} + f_i \quad , \tag{A.19}$$

where we note that, here, f_i is not the distribution function. We use this assumption at the $(i - 1)$th spatial point to replace n_{i-1}^{N+1} in the tridiagonal equation (A.13), resulting in

$$a_i \, n_{i+1}^{N+1} + (b_i + c_i \, e_{i-1}) n_i^{N+1} + c_i \, f_{i-1} = d_i \quad . \tag{A.20}$$

Comparing this to the assumption (A.19), we find the relations

$$e_i = \frac{- a_i}{b_i + c_i \, e_{i-1}} \quad \text{and} \quad f_i = \frac{d_i - c_i \, f_{i-1}}{b_i + c_i \, e_{i-1}} \quad . \tag{A.21}$$

If e_1 and f_1 ($\alpha_o = 0$ boundary) are known, all other e_i and f_i values may be generated. (Recall that all a_i, b_i, c_i, and d_i values are

known.) The boundary condition on $n(\alpha_o)$ at $\alpha_o = 0$ is $n(0) = 0$, which, with definition (1.19), requires

$$e_1 = 0 \quad , \quad f_1 = 0 \quad . \tag{A.22}$$

Using these values for starting points, we calculate all e_i and f_i values for $i = 2$ to $i = M - 1$, where M is the number of grid points used to represent the pitch-angle coordinate ($i = 1 \Rightarrow \alpha_o = 0$; $i = M \Rightarrow \alpha_o = \pi/2$). The boundary condition on $n(\alpha_o)$ at $\alpha_o = \pi/2$ is $n(\pi/2) = 0$, written as

$$n_M^{N+1} = 0 \quad . \tag{A.23}$$

Using relation (A.19) we may now generate, since all f_i and e_i values are known, all n_i values, from $i = M - 1$ to $i = 2$. Thus, for time step $N + 1$, all n_i^{N+1} values are obtainable.

We test our numerical pitch-angle diffusion scheme by following the evolution in time of an initially anisotropic distribution function ($\partial f/\partial \alpha_o \neq 0$). Figure 17 shows that after 100 time steps the distribution function is indistinguishable from isotropy.

APPENDIX II

LIMIT OF CONSTANT ISOTROPY

Our aim is to show that, for the model similar to that of Murty and Varma, in the limit of forcing the distribution to remain isotropic (infinite continuous diffusion) throughout the magnetic field cycle, there is no net momentum gain. To motivate this, we first examine the case of isotropizing at four stages (as opposed to two stages in the Alfvénic model) per cycle. The magnetic field values (equatorial) of the cycle will be

$$B_o \rightarrow B_1 \rightarrow B_2 \rightarrow B_3 = B_1 \rightarrow B_4 = B_o \quad . \tag{A.24}$$

Conserving the first adiabatic invariant as the magnetic field changes from B_o to B_1, we find

$$P_1^2 = \frac{1}{3} P_o^2 \left(2 \frac{B_1}{B_o} + 1\right) \quad , \tag{A.25}$$

and upon isotropizing, find

$$P_{\perp_1}^2 = \frac{2}{3} P_o^2 \left(2 \frac{B_1}{B_o} + 1\right) \quad , \quad P_{\parallel_1}^2 = \frac{1}{3} P_o^2 \left(2 \frac{B_1}{B_o} + 1\right) \quad . \quad \text{(A.26)}$$

The adiabatic change in field strength from B_1 to B_2 yields

$$P_2^2 = \frac{1}{3^2} P_o^2 \left(2 \frac{B_1}{B_o} + 1\right)\left(2 \frac{B_2}{B_1} + 1\right) \quad , \quad \text{(A.27)}$$

and upon isotropizing,

$$P_{\perp_2}^2 = \frac{2}{3} \frac{1}{3^2} P_o^2 \left(2 \frac{B_1}{B_o} + 1\right)\left(2 \frac{B_2}{B_1} + 1\right) \quad ,$$

$$P_{\parallel_2}^2 = \frac{1}{3} \frac{1}{3^2} P_o^2 \left(2 \frac{B_1}{B_o} + 1\right)\left(2 \frac{B_2}{B_1} + 1\right) \quad . \quad \text{(A.28)}$$

The field change from B_2 to B_3 gives

$$P_3^2 = \frac{1}{3^3} P_o^2 \left(2 \frac{B_1}{B_o} + 1\right)\left(2 \frac{B_2}{B_1} + 1\right)\left(2 \frac{B_3}{B_2} + 1\right) \quad . \quad \text{(A.29)}$$

Similarly, isotropizing and the field change from B_3 to B_4 will yield

$$P_4^2 = \frac{1}{3^4} P_o^2 \left(2\frac{B_1}{B_o} + 1\right)\left(2\frac{B_2}{B_1} + 1\right)\left(2\frac{B_3}{B_2} + 1\right)\left(2\frac{B_4}{B_3} + 1\right) \quad . \quad (A.30)$$

Assuming that $B_3 = B_1$ and $B_4 = B_o$, we find the fractional momentization per cycle to be

$$\frac{P_4}{P_o} = \frac{1}{3^2}\sqrt{5 + 2\left(\frac{B_1}{B_o} + \frac{B_o}{B_1}\right)}\sqrt{5 + 2\left(\frac{B_2}{B_1} + \frac{B_1}{B_2}\right)} \quad . \quad (A.31)$$

If the distribution is isotropized at N steps during the cycle, rather than at four, Equation (A.31) becomes

$$\frac{P_N}{P_o} = \frac{1}{3^{N/2}} \prod_{1}^{N/2} \left[5 + 2\left(\frac{B_i}{B_{i-1}} + \frac{B_{i-1}}{B_i}\right)\right]^{1/2} \quad , \quad (A.32)$$

where we have assumed $B_{(N/2)+i} = B_{(N/2)-i}$. For simplicity, we let the magnetic field strength change linearly with time from $B = B_o$ to $B = B_{N/2}$, and then decrease linearly back from $B = B_{N/2}$ to $B = B_N = B_o$. Thus, we may write (for $i \leq N/2$)

$$B_i = B_o + i\,\Delta B \quad , \quad (A.33)$$

where

$$\Delta B = \frac{B_{N/2} - B_o}{\frac{N}{2}} \quad , \tag{A.34}$$

with this, we may substitute

$$\frac{B_i}{B_{i-1}} + \frac{B_{i-1}}{B_i} = \frac{B_i}{B_i - \Delta B} + \frac{B_i - \Delta B}{B_i} \cong 2 + \left(\frac{\Delta B}{B_i}\right)^2 \tag{A.35}$$

in Equation (A.32) to get

$$\frac{P_N}{P_o} \cong \frac{1}{3^{N/2}} \prod_{1}^{N/2} \left[5 + 4 + 2\left(\frac{\Delta B}{B_i}\right)^2\right]^{-1/2} \quad . \tag{A.36}$$

Replacing B_i by $B_{MIN} = B_o$ (which will give an upper bound to $\Delta B/B_i$, hence to P_N/P_o), we may write

$$\frac{P_N}{P_o} \cong \frac{1}{3^{N/2}} \left[9 + 2\left(\frac{\Delta B}{B_o}\right)^2\right]^{-N/4} \cong \left[1 + \frac{2}{9}\left(\frac{\Delta B}{B_c}\right)^2\right]^{-N/4} \quad . \tag{A.37}$$

Using the binomial expansion, we rewrite this as

$$\frac{P_N}{P_o} \cong 1 + \frac{N}{4}\frac{1}{9}\left(\frac{\Delta B}{B_o}\right)^2 \quad . \tag{A.38}$$

Replacing ΔB with its definition, relation (A.34), the fractional momentum gain per cycle is

$$\frac{P_N}{P_o} \cong 1 + \frac{1}{N}\frac{1}{9}(1 + 2k + k^2) \quad , \tag{A.39}$$

where $k = B_{MAX}/B_{MIN} = B_{N/2}/B_o$ (Equation (23)). In the limit of $N \to \infty$ (forcing constant isotropy), we find

$$\frac{P_N}{P_o} \to 1 \quad , \tag{A.40}$$

resulting in no net momentum gain over the cycle.

ACKNOWLEDGMENTS

The authors wish to thank Alice Shank, John Birkbeck, and Jeana Wonderlich for their assistance. A special note of thanks to Larry Schroder, Dr. Richard Carlson, and the University of Iowa Nuclear Physics Group for the unlimited use of their CDC 3800 computer. This work was supported by the Atmospheric Science Section of the National Science Foundation and by NASA grants NSG-7632 and NGL-16-001-002.

REFERENCES

Alfvén, H., On the origin of cosmic radiation, Tellus, 6, 232, 1954.

Alfvén, H., and C.-G. Fälthammar, Cosmical Electrodynamics, Oxford, London, 1963.

Barbosa, D. D., D. A. Gurnett, W. S. Kurth, and F. L. Scarf, Structure and properties of Jupiter's magnetoplasma disc, Geophys. Res. Lett., 6, 785, 1979.

Barish, F. D., and R. A. Smith, An analytical model of the Jovian magnetosphere, Geophys. Res. Lett., 2, 269, 1975.

Belcher, J. W., C. K. Goertz, and H. S. Bridge, The low energy plasma in the Jovian magnetosphere, Geophys. Res. Lett., in press, 1980.

Borovsky, J. E., Magnetic pumping and the energization of magnetospheric particles, M.S. thesis, University of Iowa, 1980.

Coroniti, F. V., Dénouement of Jovian radiation belt theory, Space Sci. Rev., 17, 837, 1975.

Goertz, C. K., Jupiter's ionosphere and magnetosphere, Planet. Space Sci., 21, 1389, 1973.

Goertz, C. K., Plasma in the Jovian magnetosphere, J. Geophys. Res., 81, 2007, 1976.

Goertz, C. K., Energization of particles in Jupiter's outer magnetosphere, J. Geophys. Res., 83, 3145, 1978.

Goertz, C. K., The Jovian magnetodisk, Space Sci. Rev., 23, 319, 1979.

Goertz, C. K., D. E. Jones, B. A. Randall, E. J. Smith, and M. F. Thomsen, Evidence for open field lines in Jupiter's magnetosphere, J. Geophys. Res., 81, 3393, 1976.

Gurnett, D. A., R. R. Shaw, R. R. Anderson, and W. S. Kurth, Whistlers observed by Voyager 1: Detection of lightning on Jupiter, Geophys. Res. Lett., 6, 511, 1979.

Hill, T. W., Inertial limit on corotation, J. Geophys. Res., 84, 6554, 1979.

Lyons, L. R., R. M. Thorne, and C. F. Kennel, Pitch-angle diffusion of radiation belt electrons within the plasmasphere, J. Geophys. Res., 77, 3455, 1972.

Murty, M. S., and R. K. Varma, Acceleration of cosmic radiation, Phys. Rev., 112, 1789, 1958.

Roach, P. J., Computational Fluid Dynamics, Hermosa Publications, Albuquerque, NM, 1972.

FIGURE CAPTIONS

Figure 1. The magnetic field model, $B = B_o + 1/2\ a\ z^2$. Shown for $B_{o_{MAX}}/B_{o_{MIN}} = 10$. Note that the two fields are equal at $z = z_c$.

Figure 2. Comparison of computer-simulated results with analytical values for the Alfvénic model. P = momentum after one cycle, P_o = initial momentum, $k = B_{o_{MAX}}/B_{o_{MIN}}$. Simulation results for the continuous-diffusion model, with the diffusion coefficient chosen to give a maximum energy gain, are also displayed.

Figure 3. The number of particles in a flux tube, $n(P,\alpha_o)$, in the Alfvénic magnetic-pumping model. (a) Initial isotropic distribution, (b) distribution after adiabatic motion due to increase in magnetic field strength, (c) distribution is pitch-angle diffused to isotropy, holding B_o at $B_{o_{MAX}}$, (d) distribution after adiabatic motion due to decrease in magnetic field.

Figure 4. Computational results of continuous diffusion model. P = momentum after one cycle, P_o = initial momentum. For the parameters of our numerical treatment $\Delta = 0.282$ gives $\tau_{DIF} = \tau_{CYCLE}$.

Figure 5. Time dependence of mean momentum of distribution in the continuous diffusion model.

Figure 6. Steady-state distribution function for a momentum-independent diffusion coefficient.

Figure 7. Steady-state distribution functions for momentum-dependent diffusion coefficients. (a) Coefficient linearly decreases such that the energization process is less efficient at higher momenta. (b) Coefficient linearly increases such that the energization process is more efficient at higher momenta. (c) Diffusion coefficient with discontinuity such that the energization process is more efficient at lower momenta. Note irregularity in vicinity of discontinuity. (d) Diffusion coefficient with discontinuity such that the energization process is more efficient at higher momenta. Definite two-temperature appearance. (Note (d) is semi-log.)

Figure 8. Models used to approximate the Jovian magnetosphere. Barish-Smith for dayside, Goertz et al. for magnetotail.

Figure 9. Corotational electrical potentials in the Jovian magnetosphere. Calculated using the magnetic field model of Figure 8.

Figure 10. Magnetic ratio $k = B_{O_{MAX}}/B_{O_{MIN}}$ in the Jovian magnetosphere as a function of the dayside radius.

Figure 11. Energization times τ_E (for various amounts of diffusion) and radial diffusion loss times τ_{RD} as functions of the Jovian dayside radius. Energization is predicted in regions where τ_E is less than τ_{RD}.

Figure 12. Jovian pitch-angle distributions, (a) for various amounts of diffusion per orbit and (b) for increased diffusion in various magnetosphere regions. Pitch-angle independent diffusion coefficients were used.
$k = B_{O_{MAX}}/B_{O_{MIN}} = 4.$

Figure 13. Pitch-angle diffusion coefficient modeled for electron resonances with whistler modes or ion resonances with ion-cyclotron modes.

Figure 14(a). Steady-state distribution functions for wave-particle diffusion coefficient. In the case of electrons interacting with whistler modes, the transition region corresponds to electron kinetic energies of from 1.1 to 3.5 KeV. In the case of ions interacting with ion-cyclotron modes, the transition region corresponds to ion (any species) kinetic energies of from 10.9 to 34.3 KeV. (b) Time development of distribution function using wave resonance diffusion coefficient.

Figure 15. Schematic overview of outer magnetosphere with magnetic-pumping process transporting ions outward and electrons inward.

Figure 16. The momentum-pitch-angle phase-space grid. Distribution at $(P^{NEW}, \alpha_o^{NEW})$ is divided between the four solid points.

Figure 17. Time action of the pitch-angle diffusion equation. Note the conformity of the large time result to the exact solution, $n(\alpha) = (\text{constant}) \sin \alpha \cos \alpha \, T(\alpha)$ corresponding to isotropy.

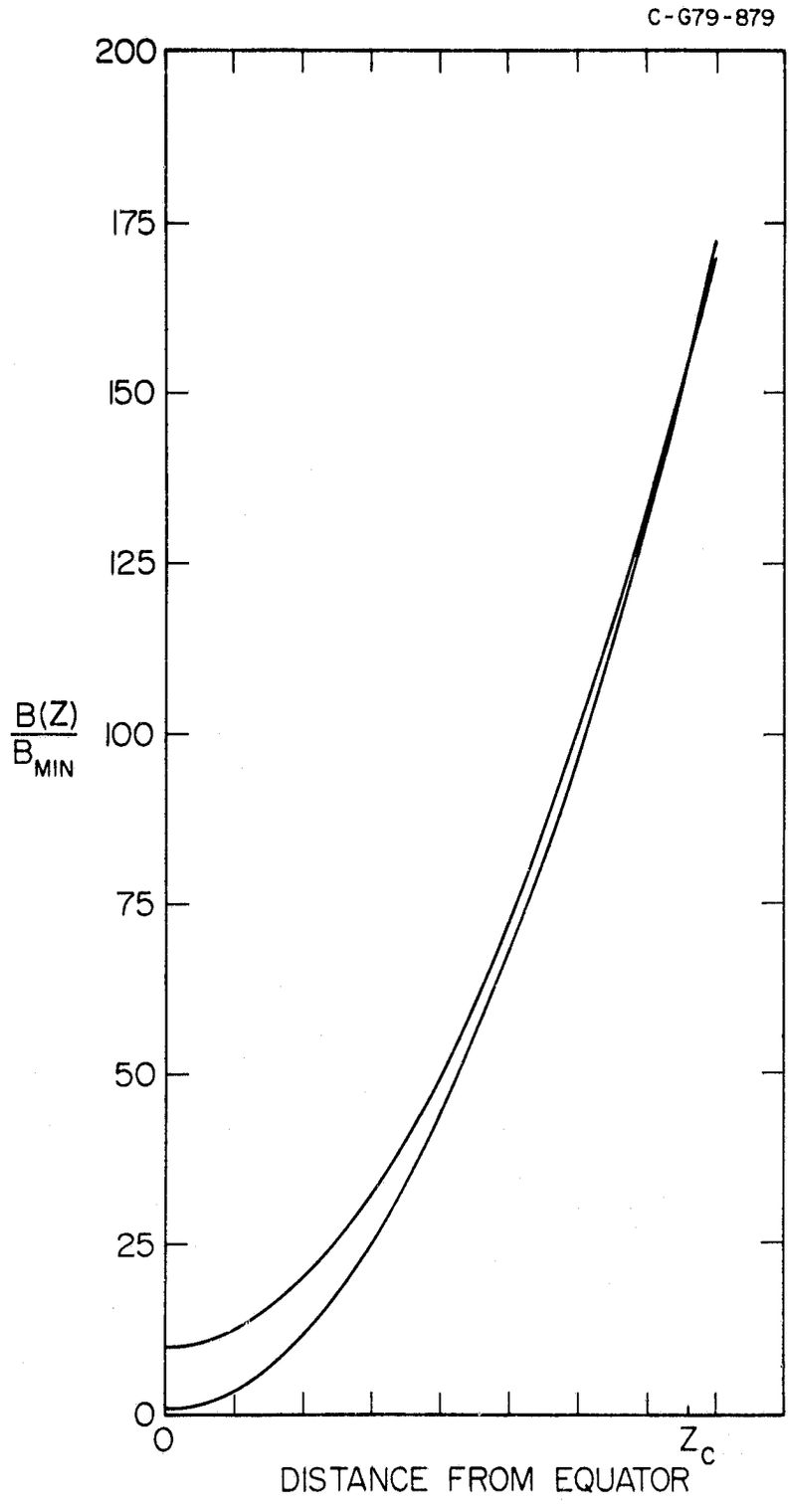
C-G79-879
200
175
150
125
100
75
50
25
0
B(Z)
B_MIN
0
Z_C
DISTANCE FROM EQUATOR

Figure 1

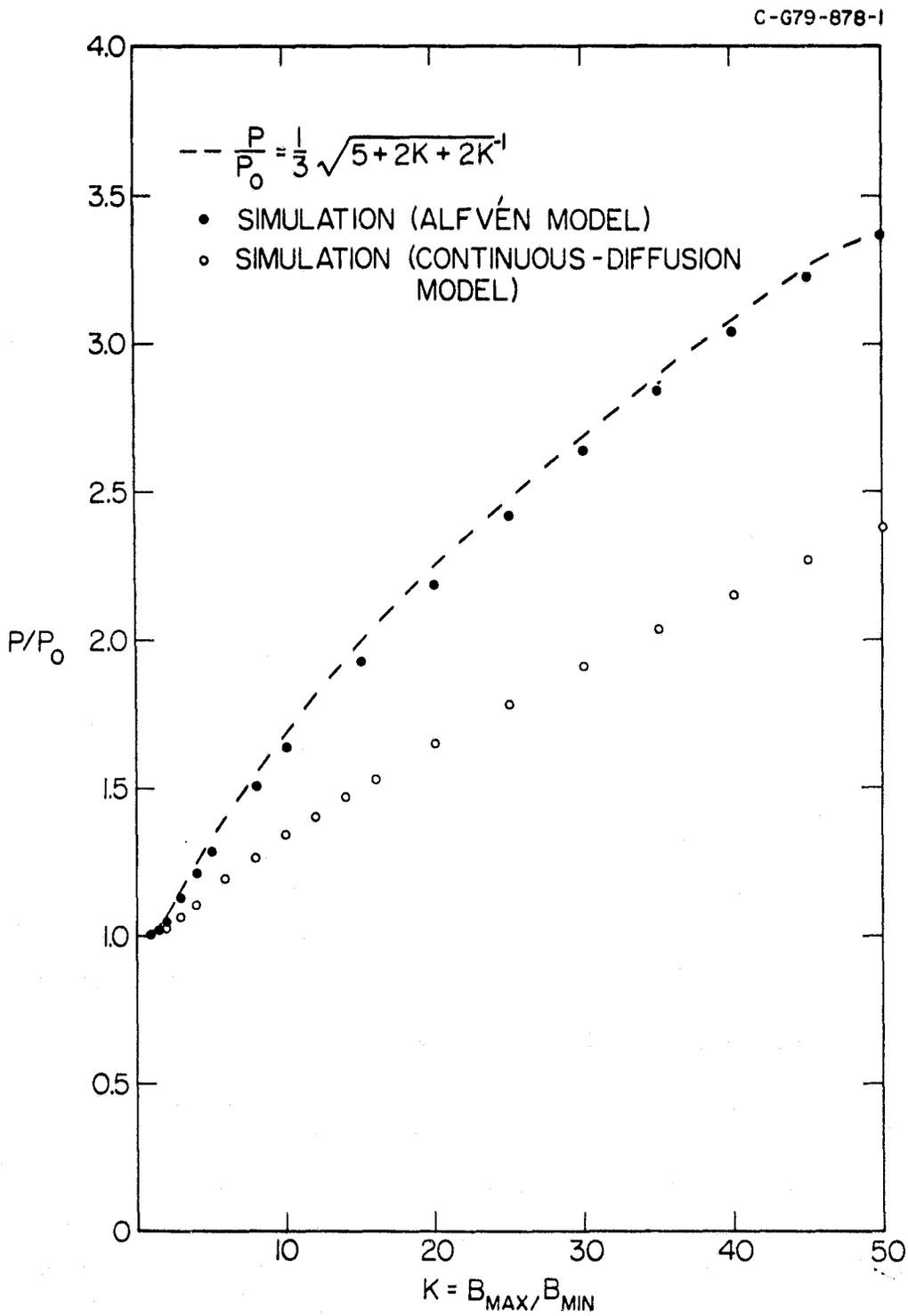
C-G79-878-I
$\frac{P}{P_0} = \frac{1}{3}\sqrt{5+2K+2K^{-1}}$
SIMULATION (ALFVÉN MODEL)
SIMULATION (CONTINUOUS-DIFFUSION MODEL)
P/P0
K = BMAX/BMIN
4.0
3.5
3.0
2.5
2.0
1.5
1.0
0.5
0
10
20
30
40
50

Figure 2

C-G79-957

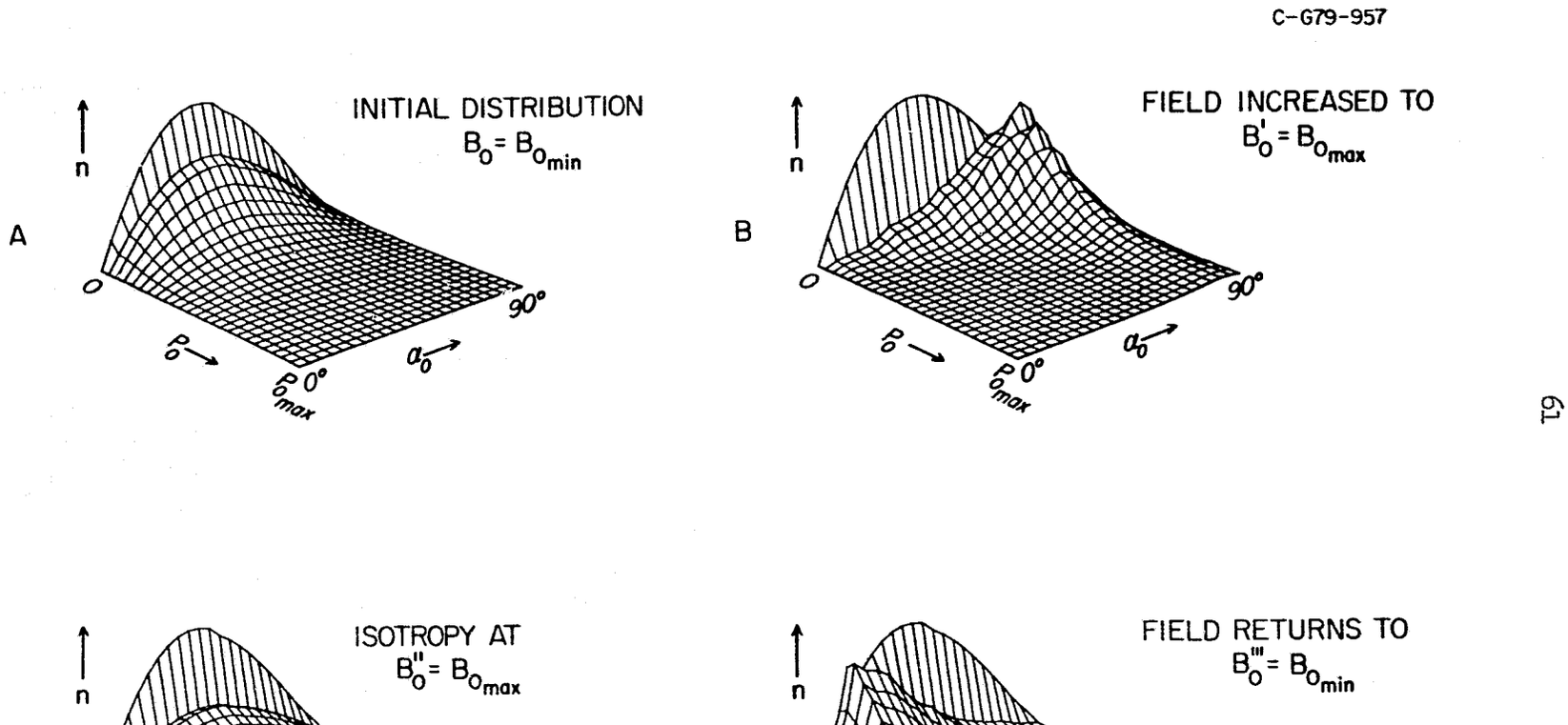

Figure 3

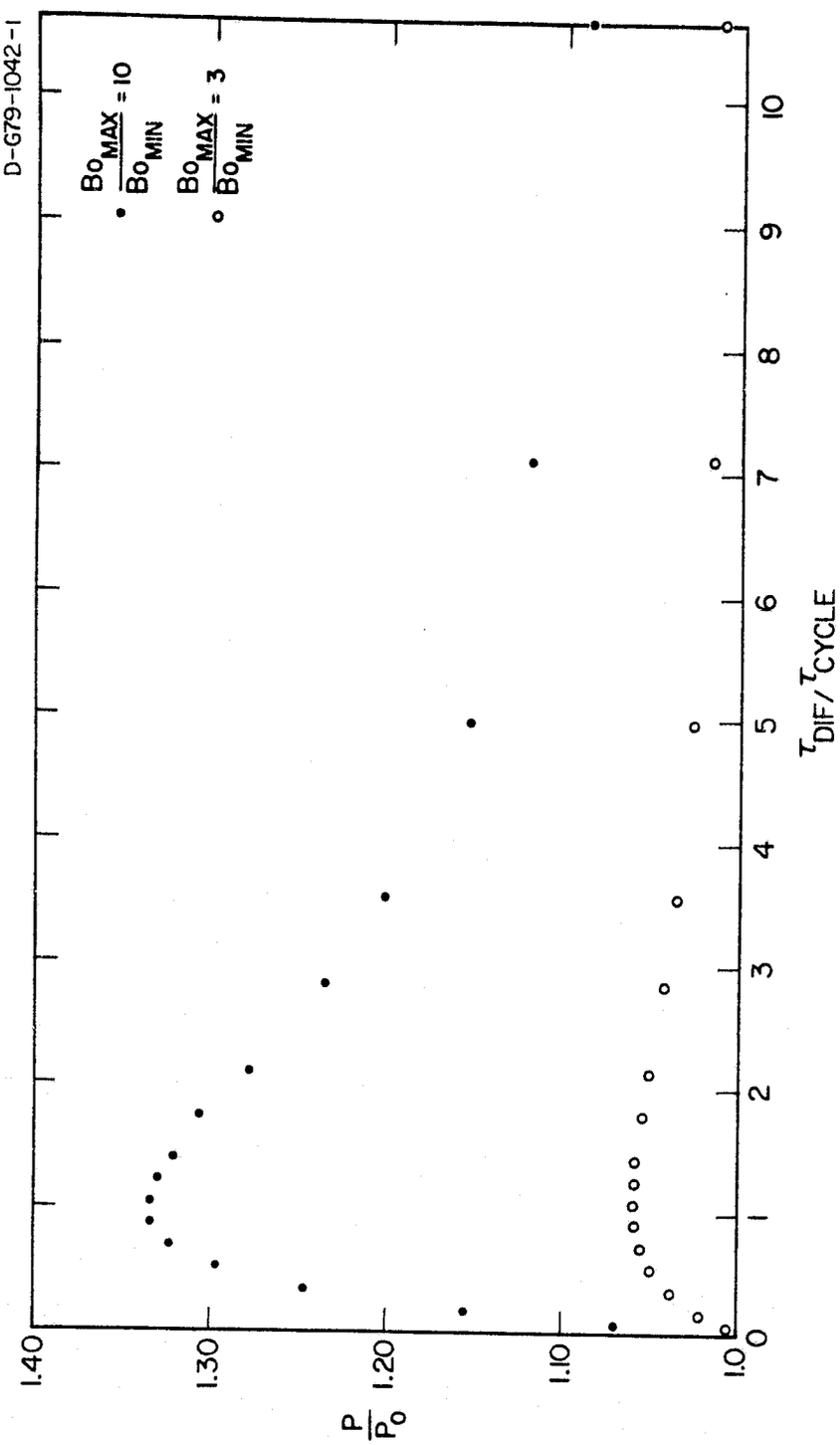
D-679-1042-1
$\frac{Bo_{MAX}}{Bo_{MIN}} = 10$
$\frac{Bo_{MAX}}{Bo_{MIN}} = 3$
$\frac{P}{P_o}$
1.40
1.30
1.20
1.10
1.0
0
1
2
3
4
5
6
7
8
9
10
τ_{DIF}/τ_{CYCLE}

Figure 4

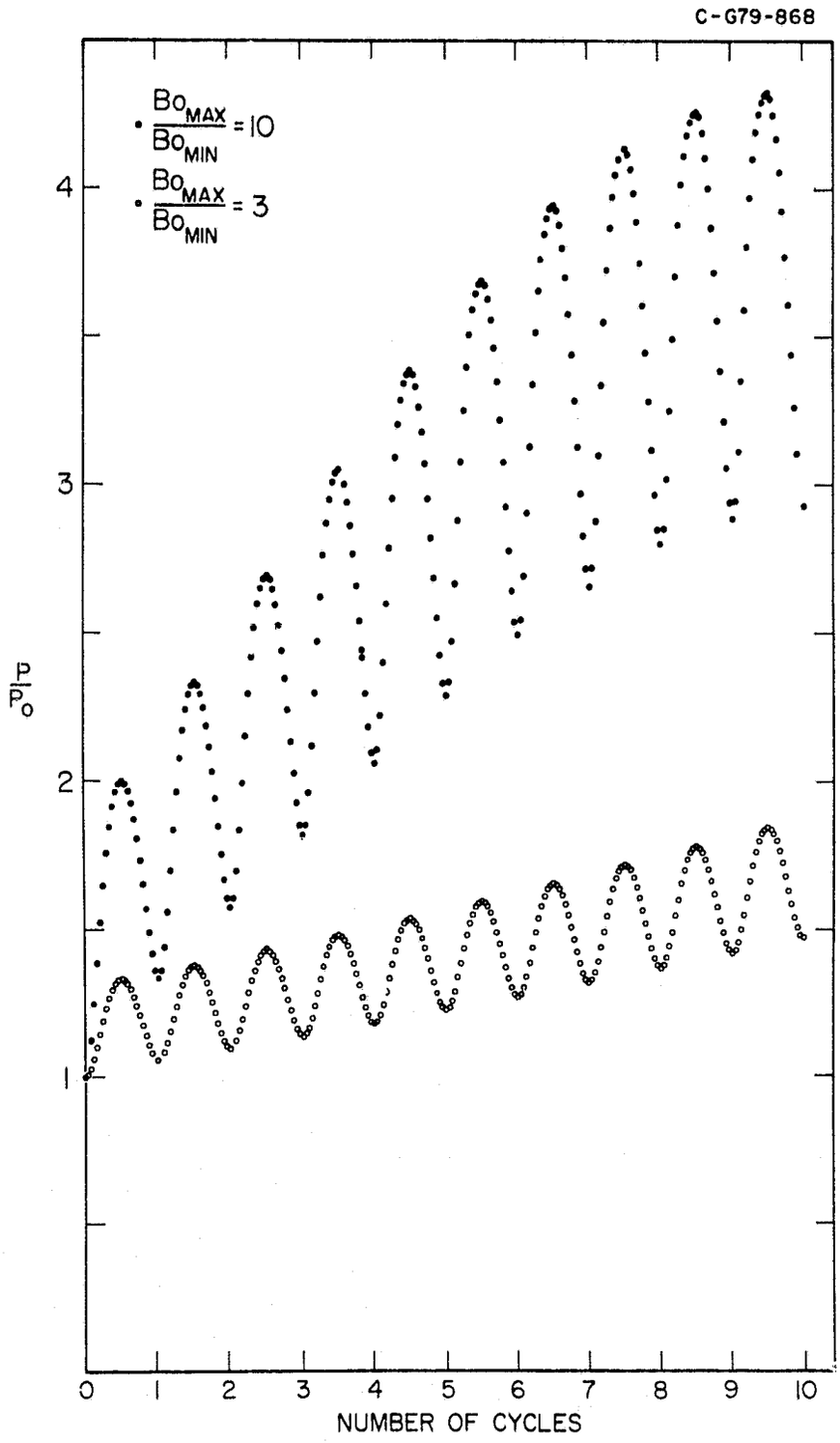
C-G79-868
$\frac{Bo_{MAX}}{Bo_{MIN}} = 10$
$\frac{Bo_{MAX}}{Bo_{MIN}} = 3$
$\frac{P}{P_o}$
1
2
3
4
0
1
2
3
4
5
6
7
8
9
10
NUMBER OF CYCLES

Figure 5

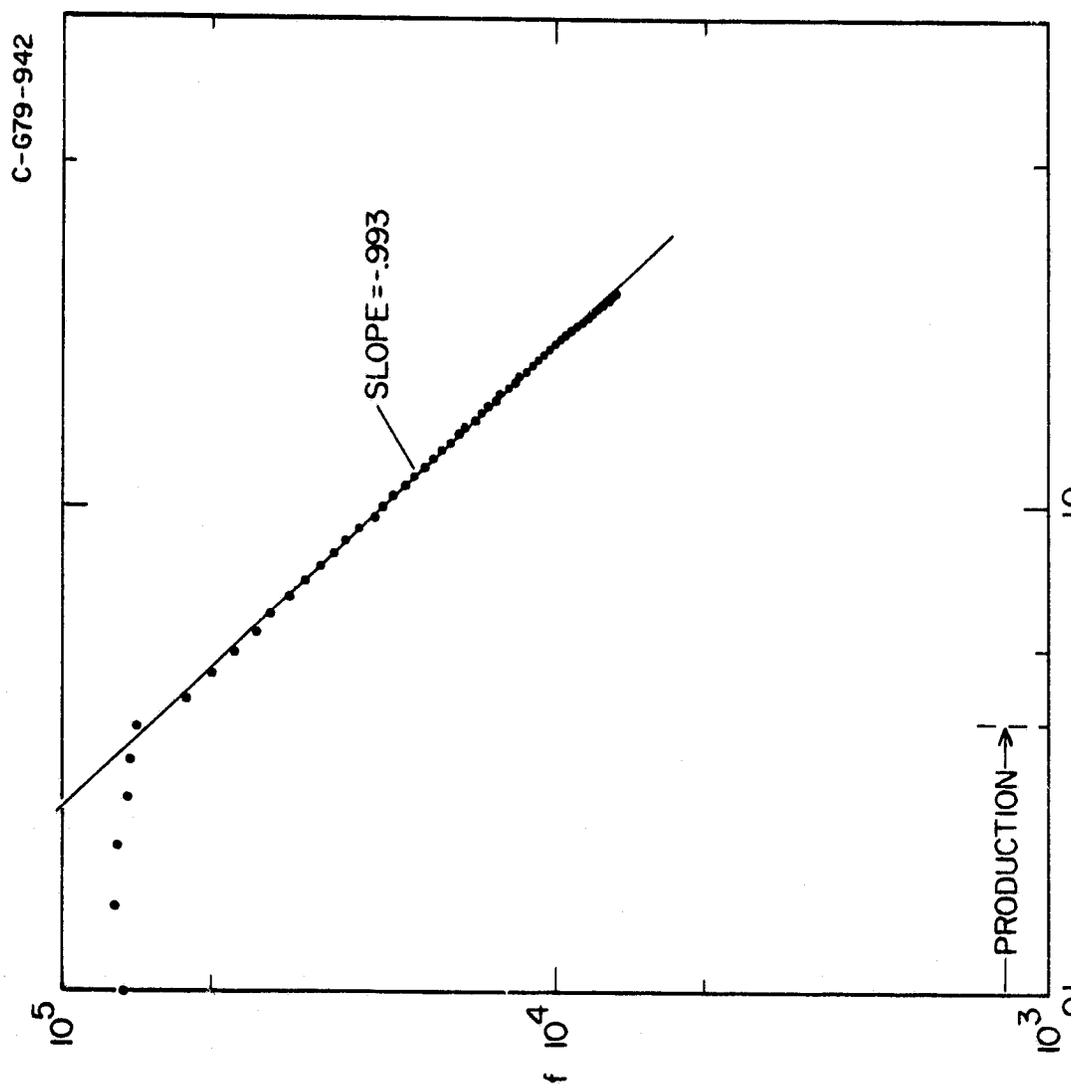

Figure 6

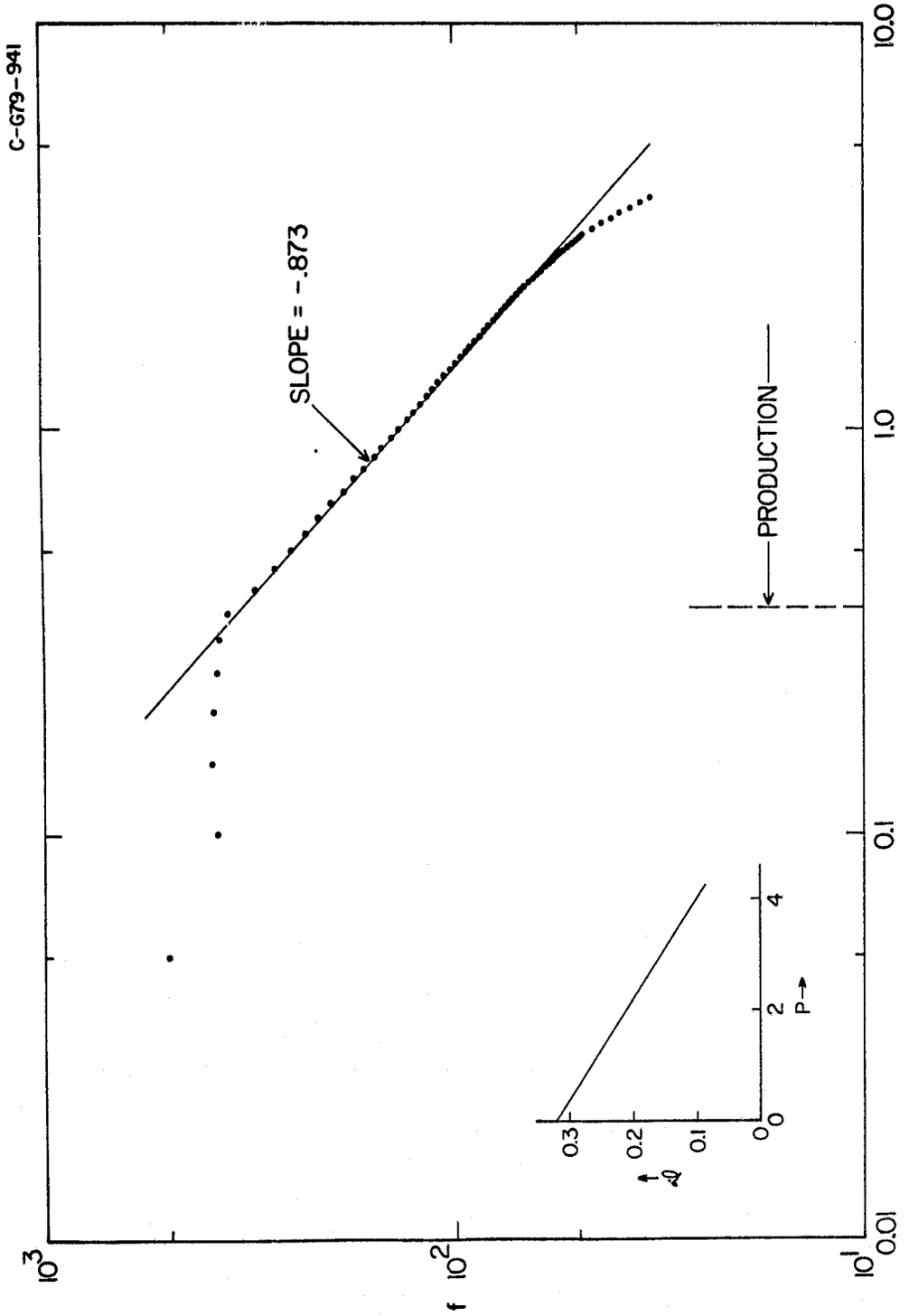
C-679-941
SLOPE = -.873
PRODUCTION
f
P
10^3
10^2
10^1
0.01
0.1
1.0
10.0
0.3
0.2
0.1
0
0
2
4
P→

Figure 7(a)

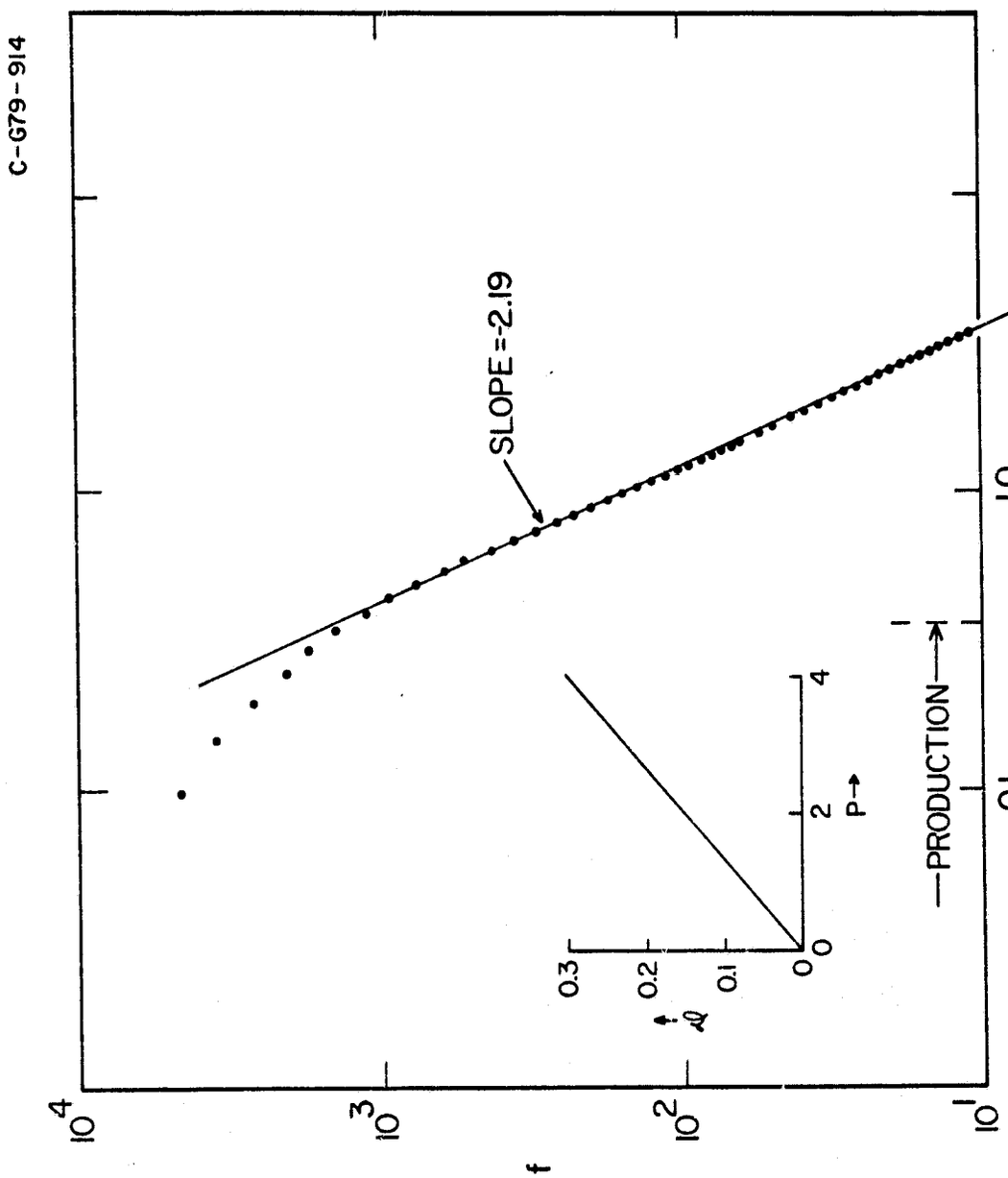
C-G79-914
SLOPE=-2.19
PRODUCTION
f
P
Q
P→
0.3
0.2
0.1
0
0
2
4
0.1
1.0
1
10^4
10^3
10^2
10^1

Figure 7(b)

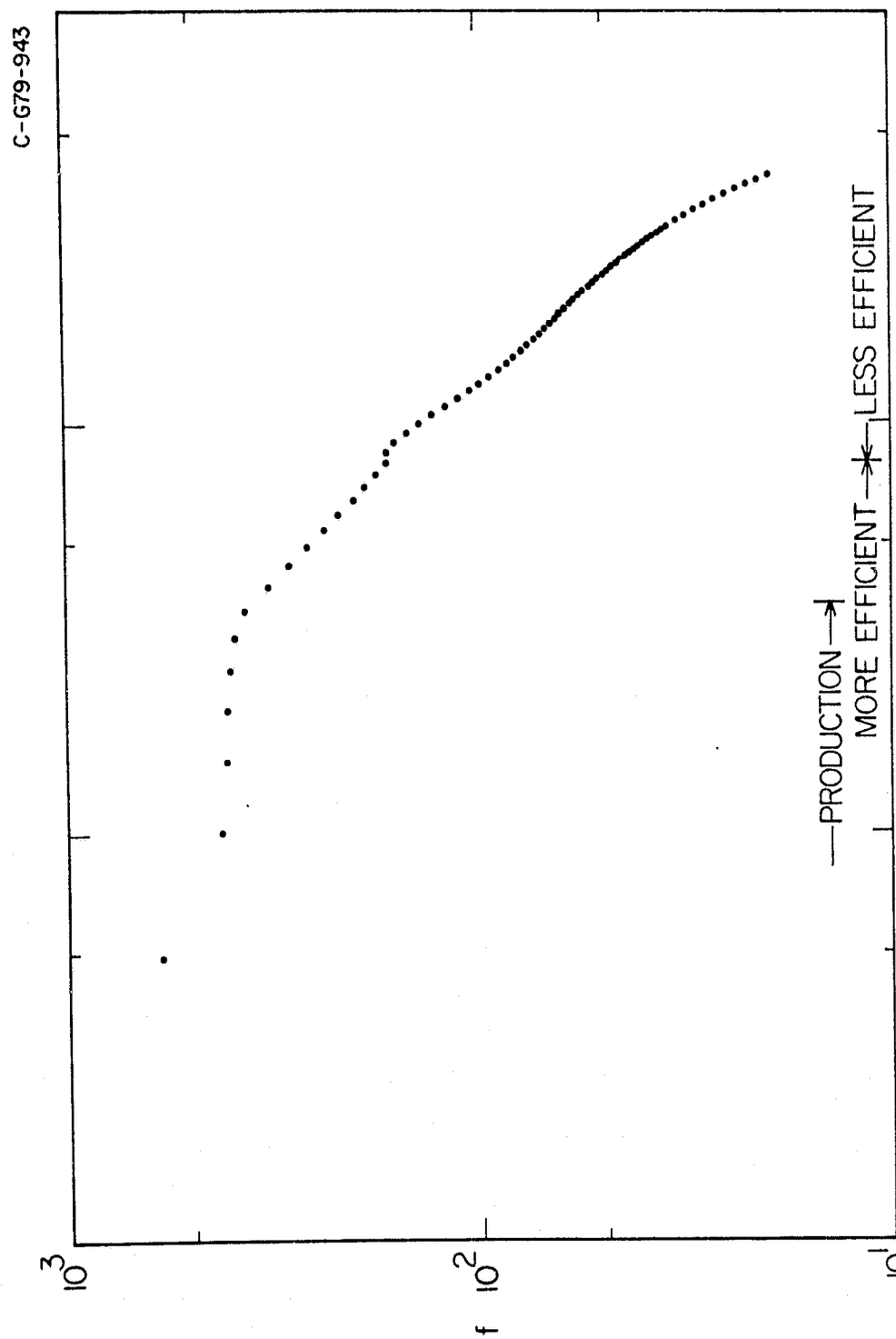
C-G79-943
10^3
10^2
10^1
f
0.1
1.0
P
—PRODUCTION→
MORE EFFICIENT →
← LESS EFFICIENT

Figure 7(c)

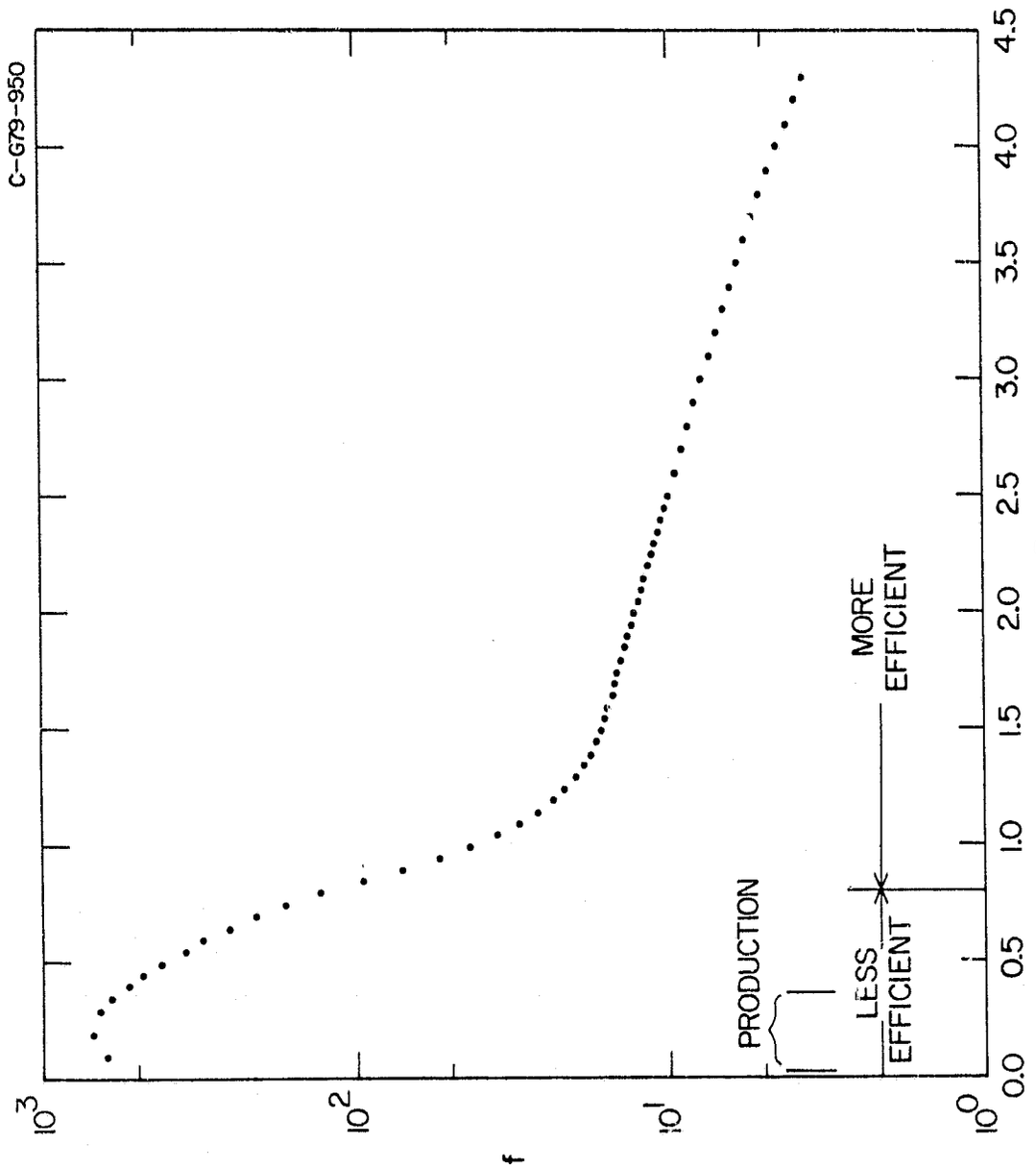
C-679-950
10^3
10^2
10^1
10^0
f
0.0
0.5
1.0
1.5
2.0
2.5
3.0
3.5
4.0
4.5
P
PRODUCTION
LESS EFFICIENT
MORE EFFICIENT

Figure 7(d)

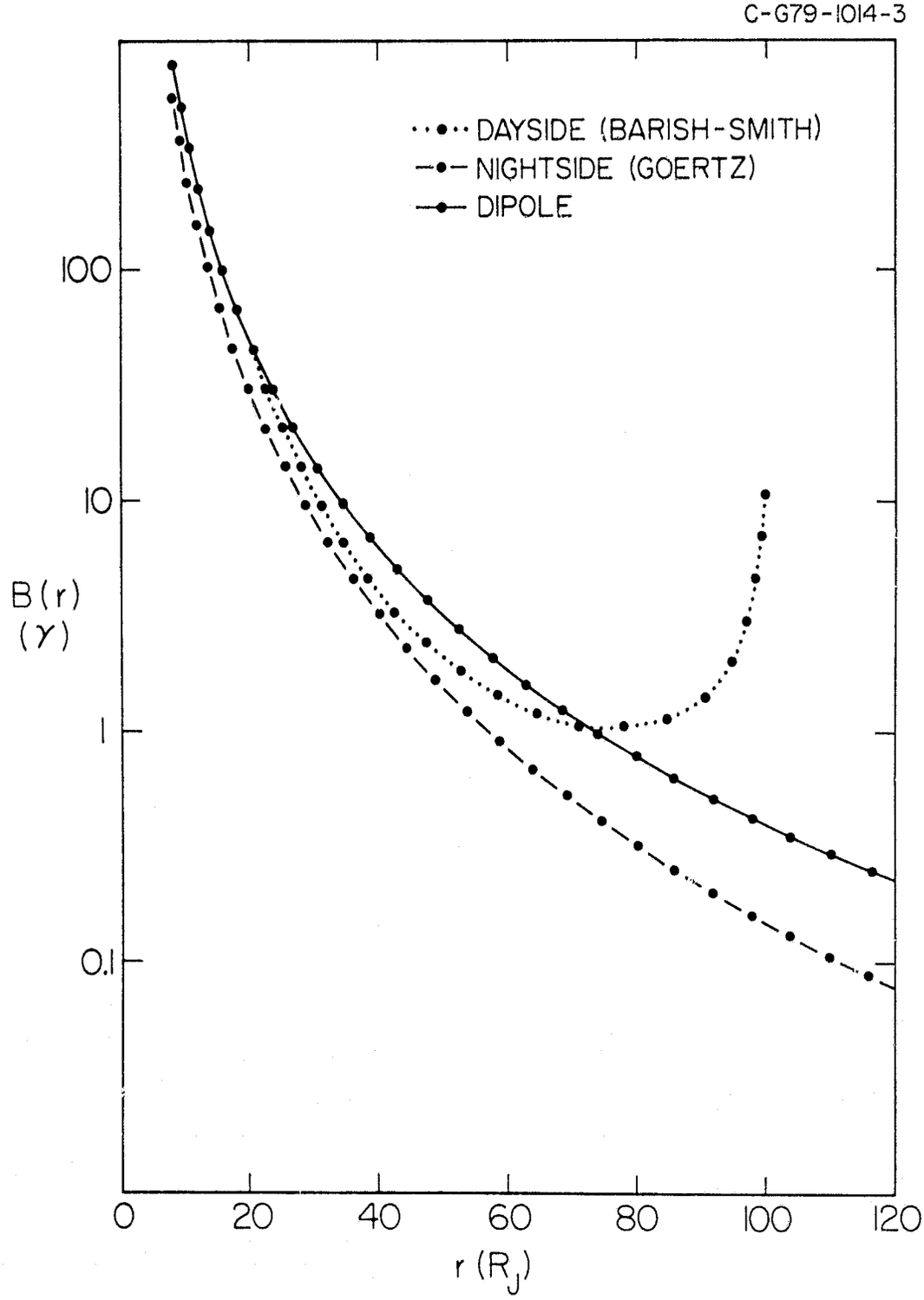
C-G79-1014-3
DAYSIDE (BARISH-SMITH)
NIGHTSIDE (GOERTZ)
DIPOLE
100
10
1
0.1
B(r)
(γ)
0
20
40
60
80
100
120
r (R_J)

Figure 8

C-G79-977-2

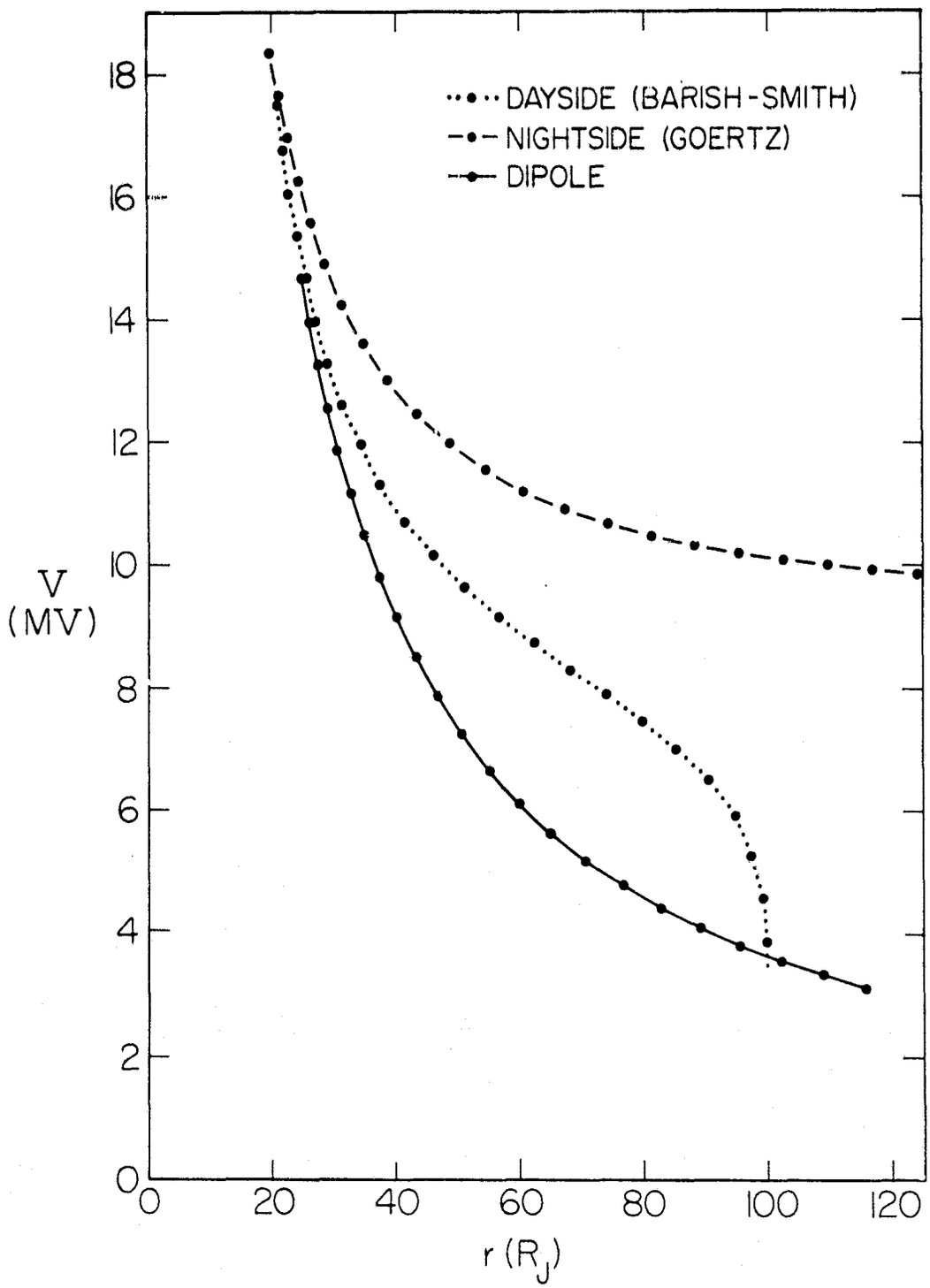

Figure 9

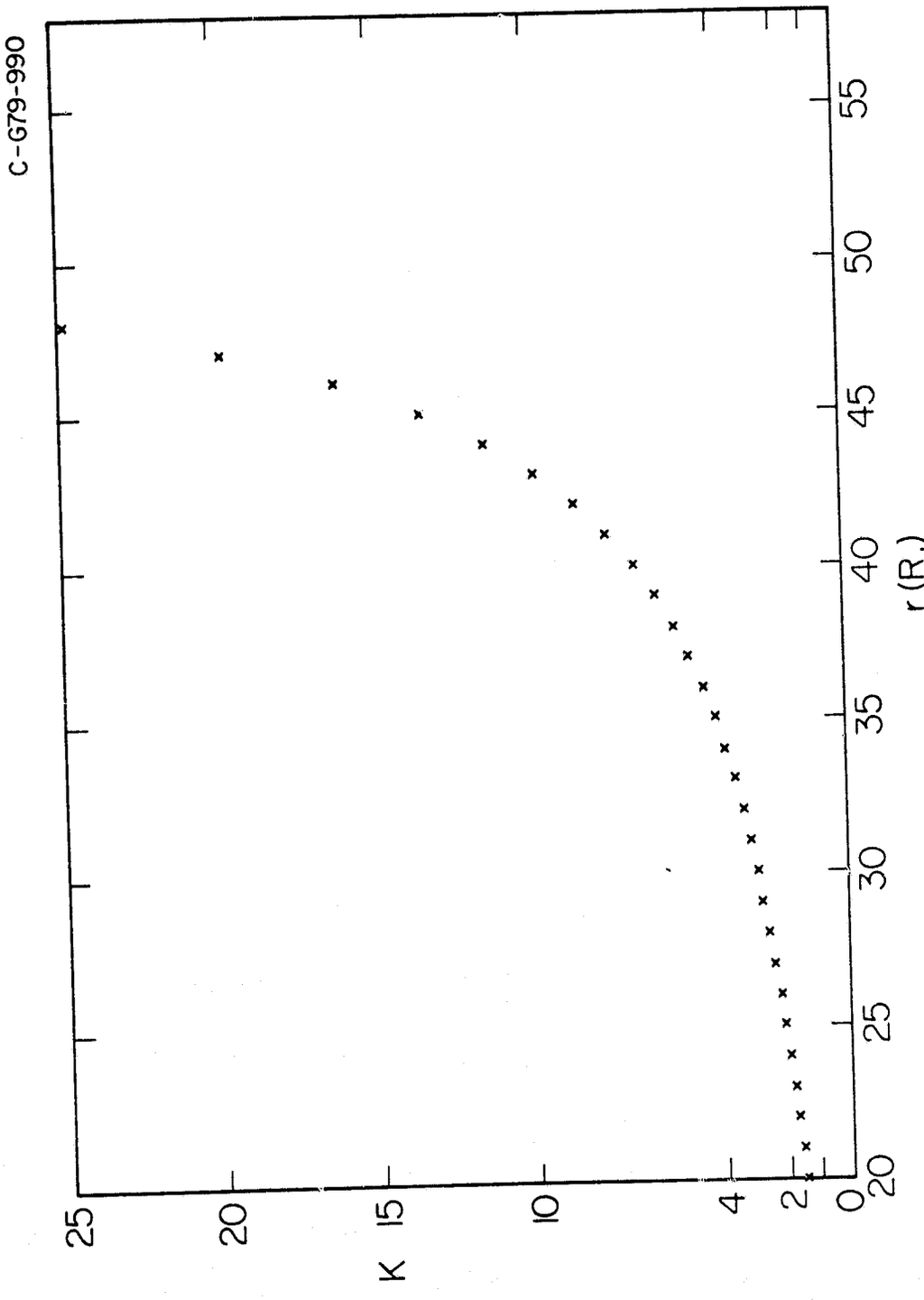

Figure 10

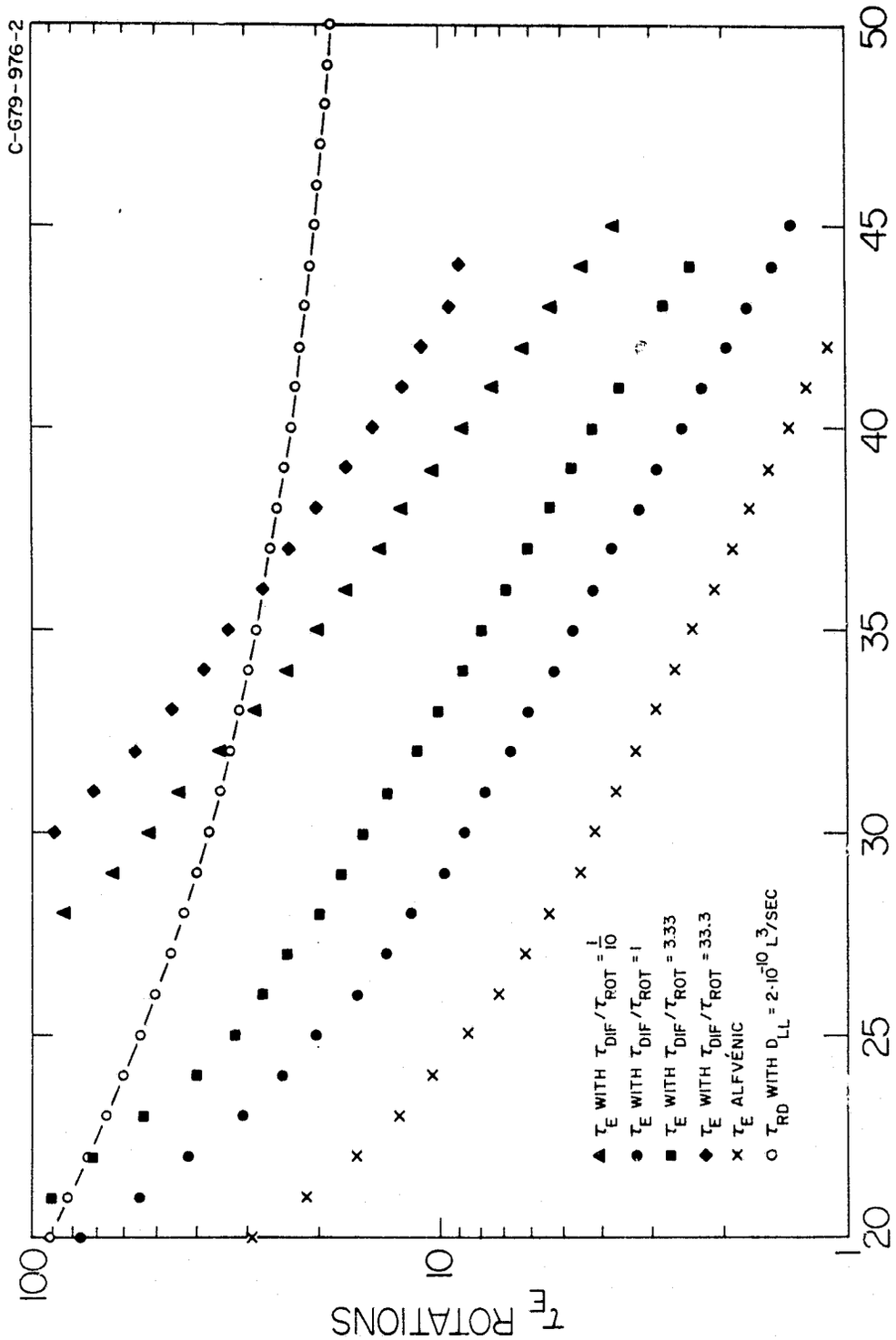
C-G79-976-2
100
10
1
τ_E ROTATIONS
20
25
30
35
40
45
50
r/R$_J$
▲ τ_E WITH $\tau_{DIF}/\tau_{ROT} = \frac{1}{10}$
● τ_E WITH $\tau_{DIF}/\tau_{ROT} = 1$
■ τ_E WITH $\tau_{DIF}/\tau_{ROT} = 3.33$
◆ τ_E WITH $\tau_{DIF}/\tau_{ROT} = 33.3$
× τ_E ALFVÉNIC
○ τ_{RD} WITH $D_{LL} = 2 \cdot 10^{10}$ L^3/SEC

Figure 11

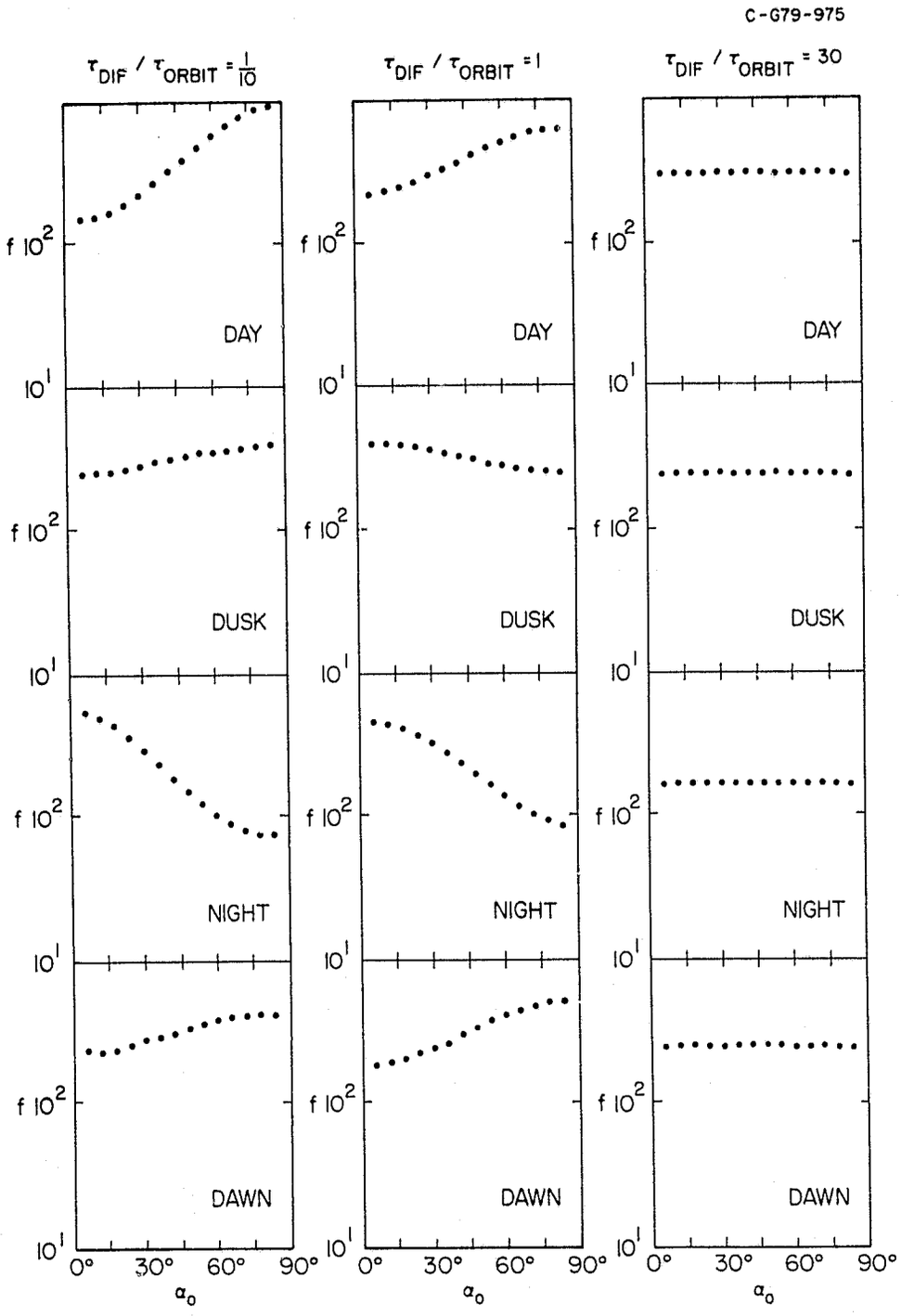
C-G79-975
$\tau_{DIF} / \tau_{ORBIT} = \frac{1}{10}$
$\tau_{DIF} / \tau_{ORBIT} = 1$
$\tau_{DIF} / \tau_{ORBIT} = 30$
f 10^2
10^1
DAY
DUSK
NIGHT
DAWN
0°
30°
60°
90°
α_0

Figure 12(a)

C-G79-994 -I

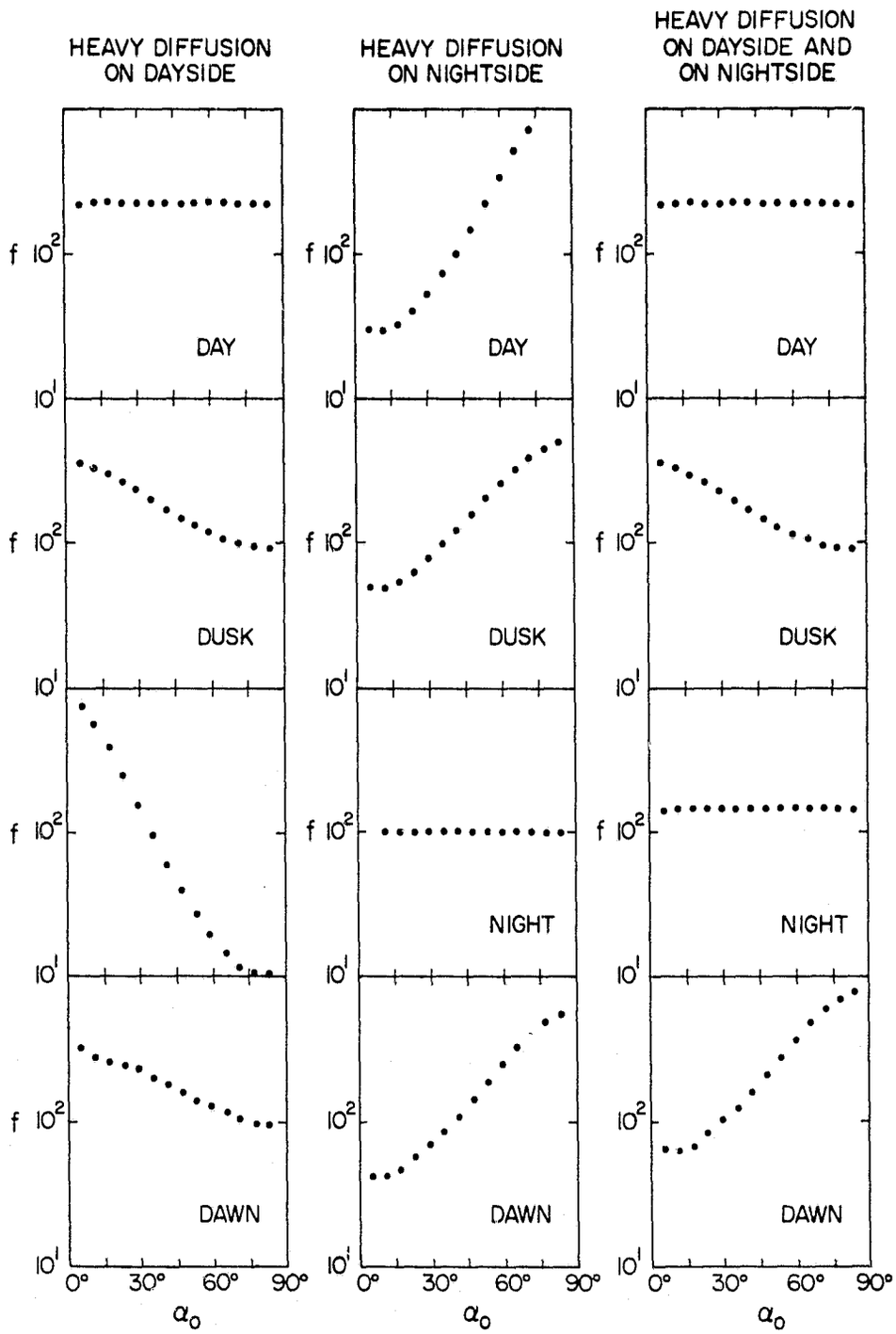

Figure 12(b)

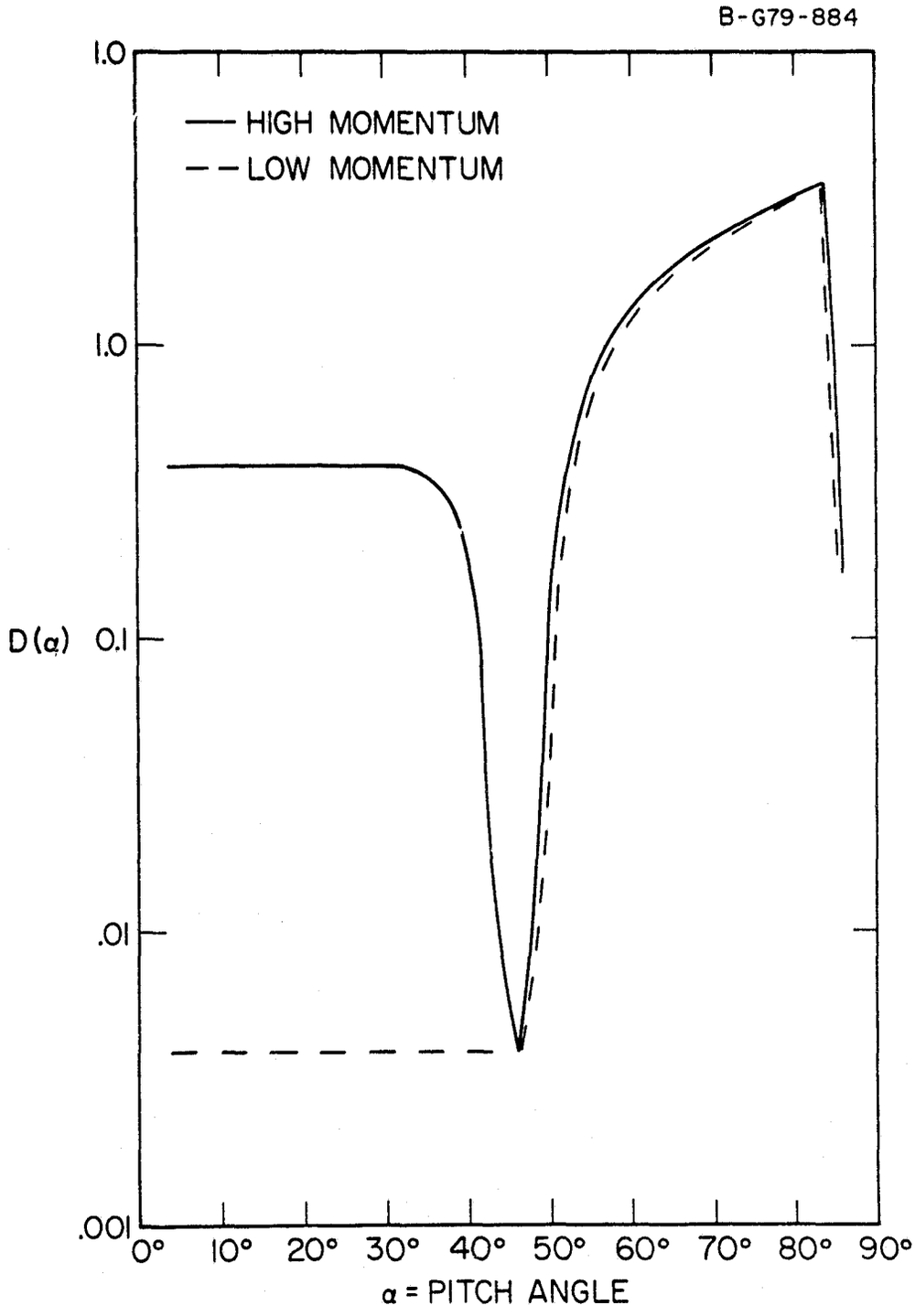
B-G79-884
1.0
HIGH MOMENTUM
LOW MOMENTUM
1.0
D(α) 0.1
.01
.001
0°
10°
20°
30°
40°
50°
60°
70°
80°
90°
α = PITCH ANGLE

Figure 13

C-G79-959

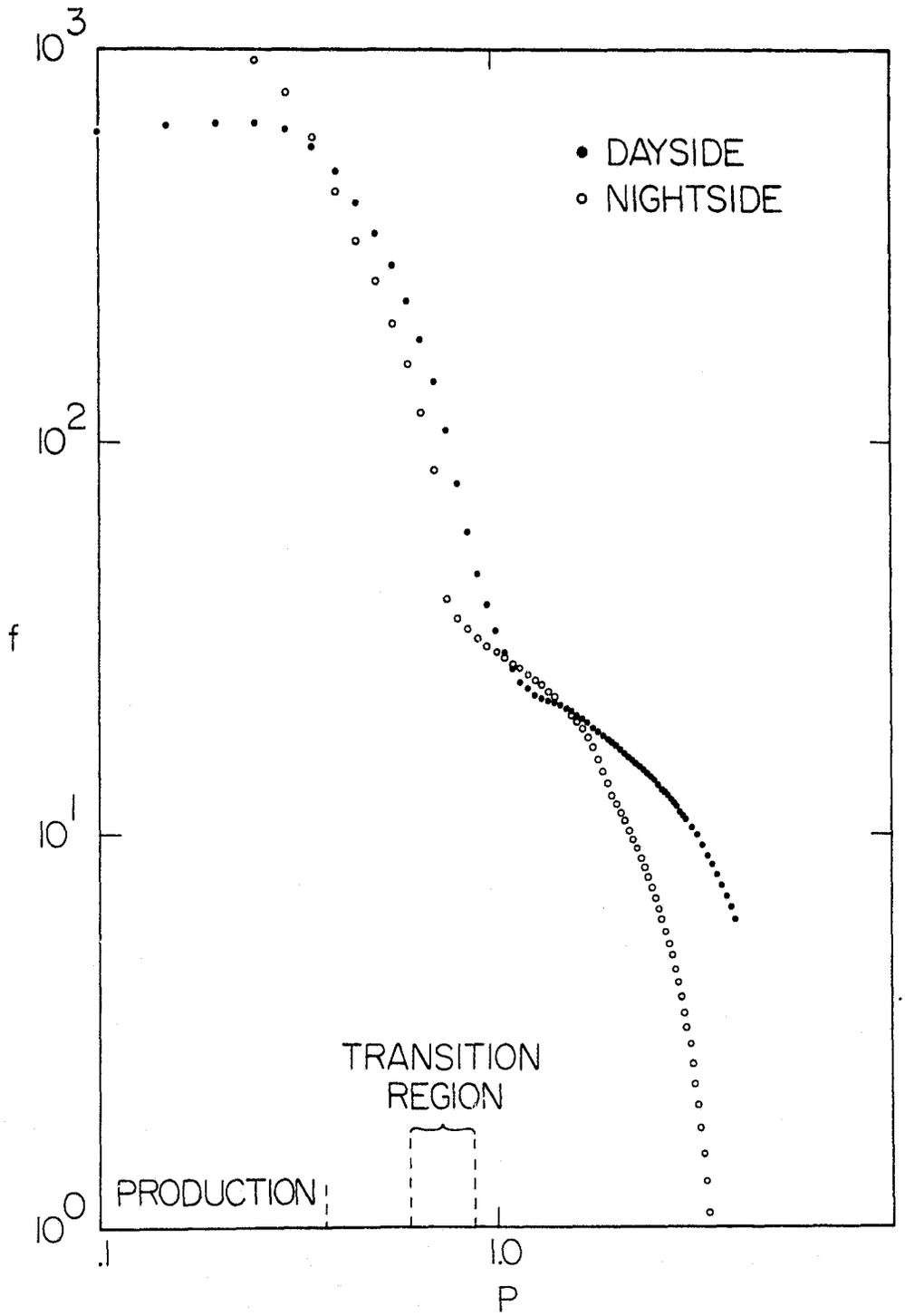

Figure 14(a)

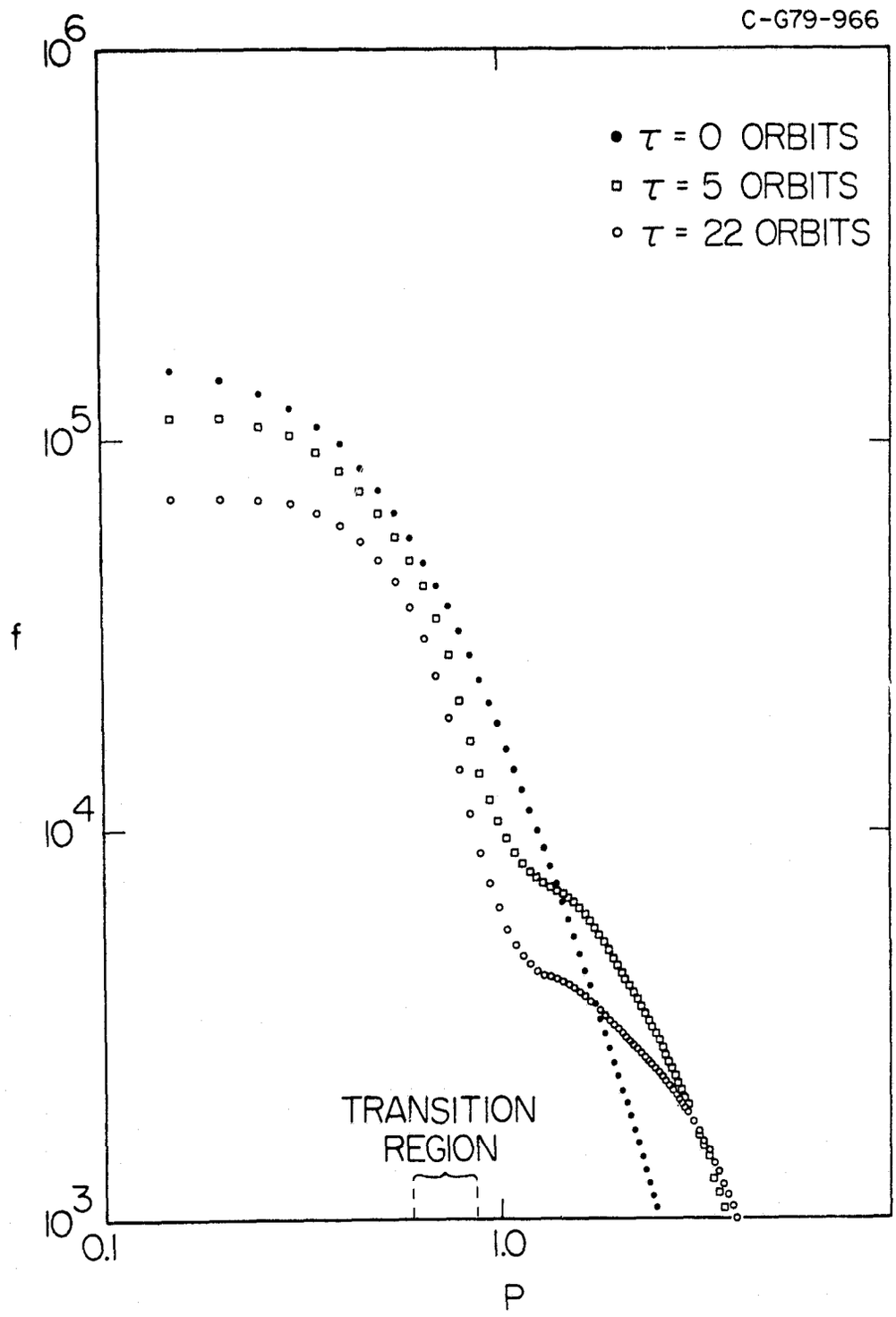
C-G79-966
10^6
10^5
10^4
10^3
f
• τ = 0 ORBITS
▫ τ = 5 ORBITS
◦ τ = 22 ORBITS
TRANSITION
REGION
0.1
1.0
P

Figure 14(b)

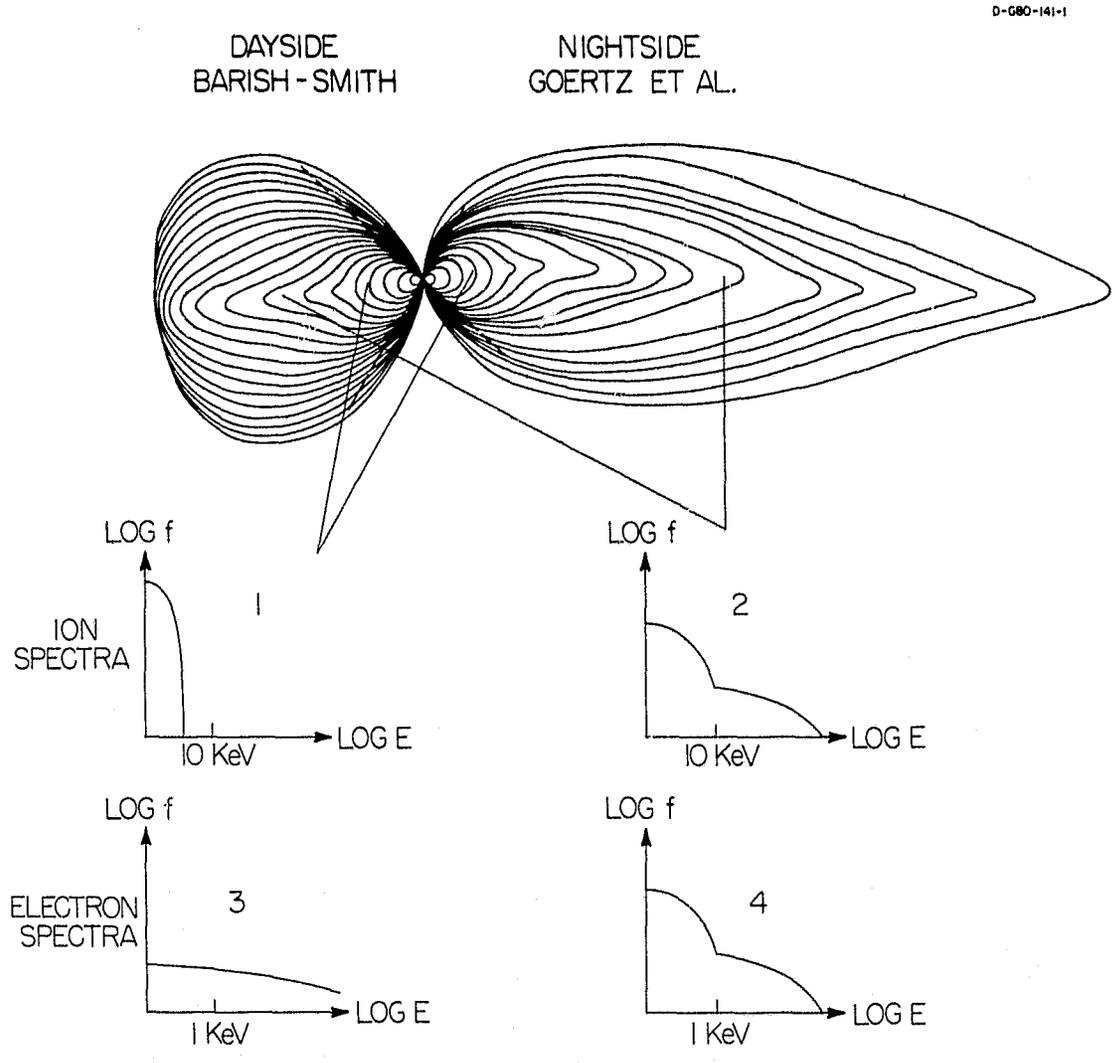
D-G80-141-1
DAYSIDE
BARISH - SMITH
NIGHTSIDE
GOERTZ ET AL.
LOG f
ION
SPECTRA
1
LOG E
10 KeV
LOG f
2
LOG E
10 KeV
LOG f
ELECTRON
SPECTRA
3
LOG E
1 KeV
LOG f
4
LOG E
1 KeV

Figure 15

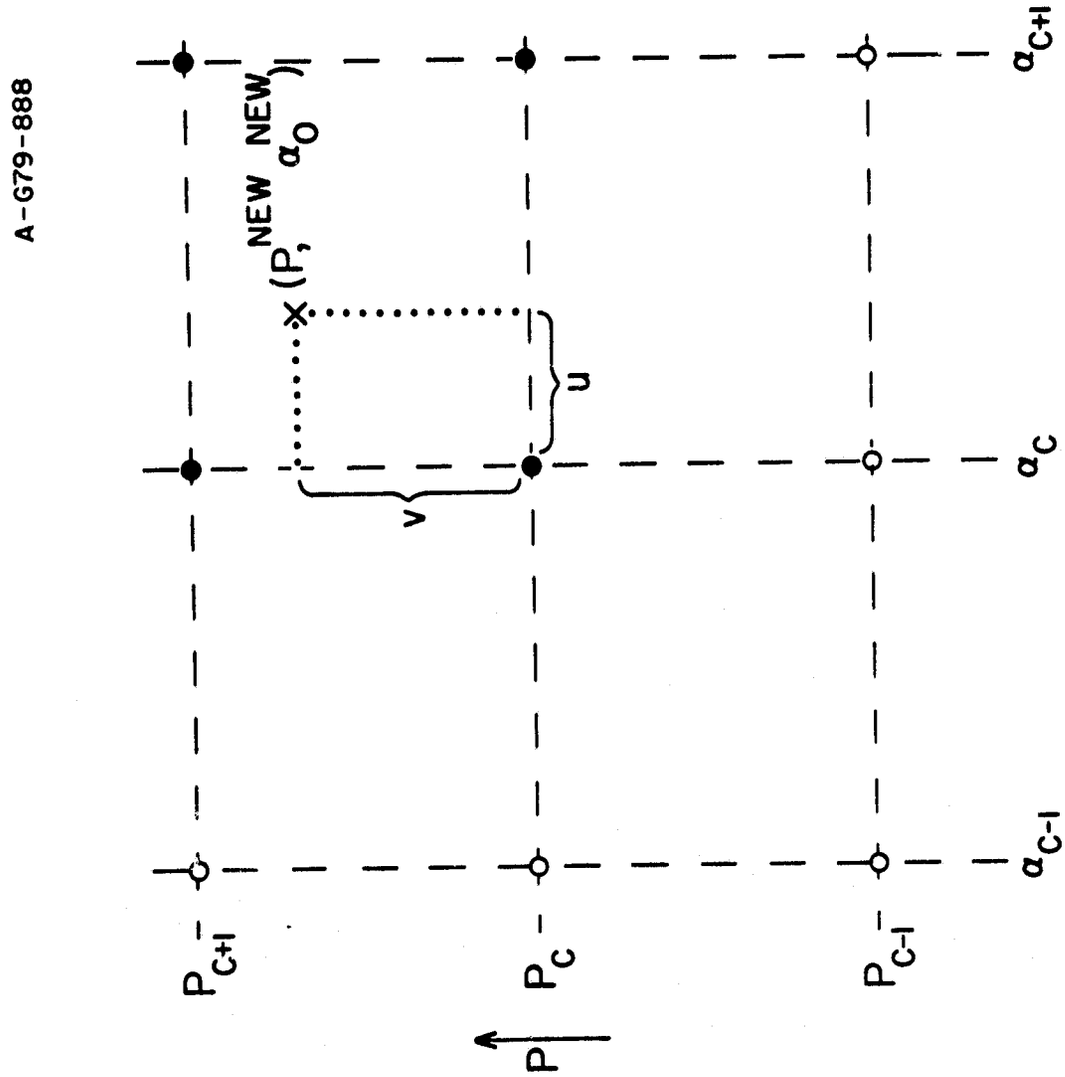
A-G79-888
$(P, \alpha_O)^{NEW}_{NEW}$
u
v
α_{C+1}
α_C
α_{C-1}
P^-_{C+1}
P^-_C
P^-_{C-1}
P
α

Figure 16

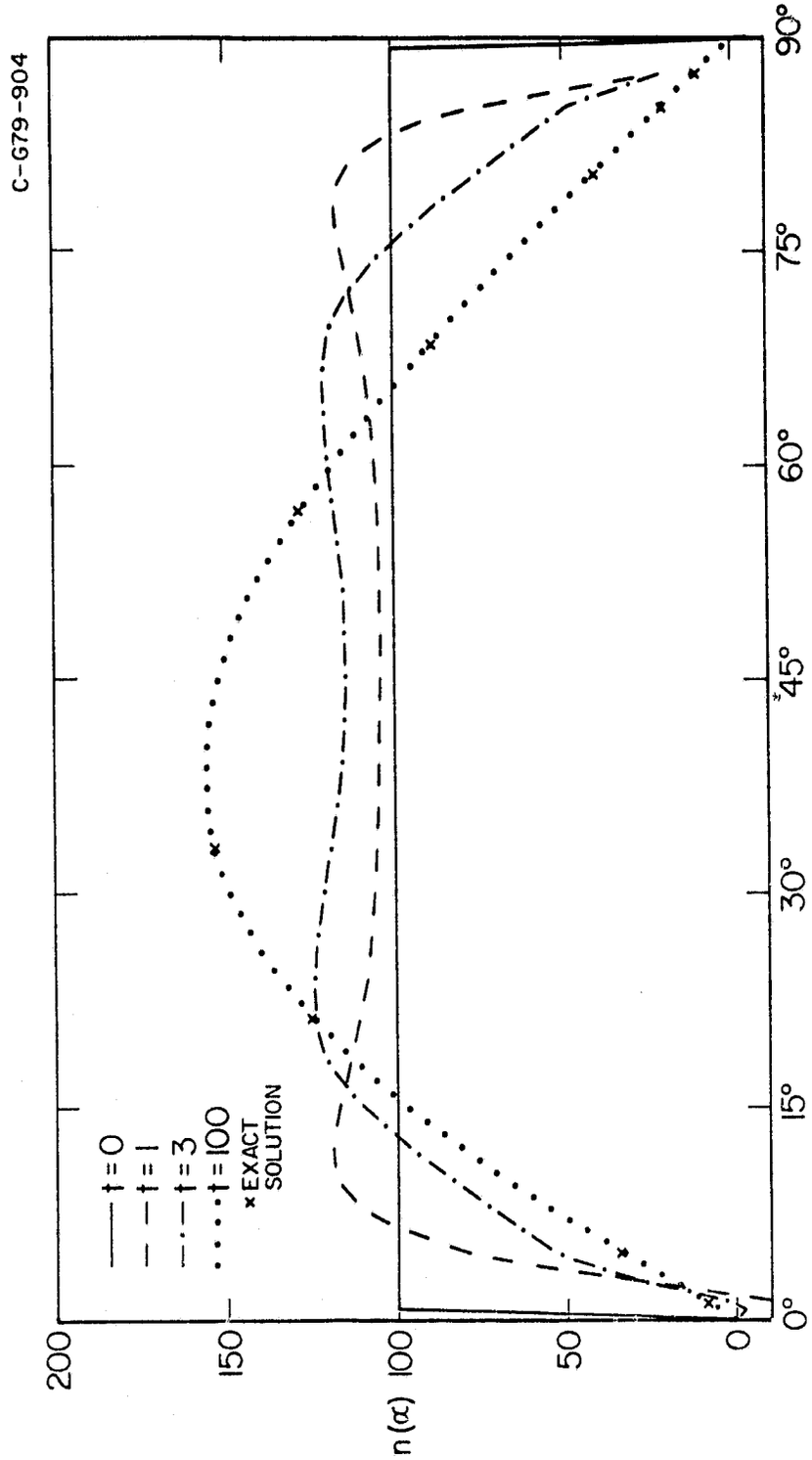
C-679-904
t=0
t=1
t=3
t=100
×EXACT SOLUTION
n(α)
200
150
100
50
0
0°
15°
30°
45°
60°
75°
90°
α

Figure 17